UNCLASSIFIED

AD NUMBER

AD391513

CLASSIFICATION CHANGES

TO: unclassified

FROM: confidential

LIMITATION CHANGES

TO:

Approved for public release, distribution unlimited

FROM:

Distribution: USGO: others to Director, Naval Research Lab., Washington, D. C. 20390.

AUTHORITY

NRL ltr. code 5304, 9 Sep 96; NRL ltr. code 5304, 9 Sep 96

THIS PAGE IS UNCLASSIFIED

SECRET

NRL Memorandum Report 1874
Copy No. [redacted] Copies

AD391513

Ocean Surveillance Radar Parametric Analysis

Case II - Noncoherent Sidelooking Radar

[Unclassified Title]

S. ANGYAL, D. F. HEMENWAY, AND S. A. ZURO

Aerospace Radar Branch
Radar Division

April 1968

DDC
RECEIVED
AUG 1 1968

NAVAL RESEARCH LABORATORY
Washington, D.C.

SECRET

Downgraded at 12 year intervals;
Not automatically declassified.

SEE INSIDE OF FRONT COVER FOR DISTRIBUTION RESTRICTIONS

SECURITY

This document contains information affecting the national defense of the United States within the meaning of the Espionage Laws, Title 18, U.S.C., Sections 793 and 794. The transmission or revelation of its contents in any manner to an unauthorized person is prohibited by law.

In addition to security requirements which apply to this document and must be met, each transmittal outside the agencies of the U.S. Government must have prior approval of the Director, Naval Research Laboratory, Washington, D.C. 20390.

OCEAN SURVEILLANCE RADAR PARAMETRIC ANALYSIS

CASE II - NONCOHERENT SIDELOOKING RADAR

(Unclassified Title)

ABSTRACT

(S) A computer-aided analysis of the Noncoherent Sidelooking Radar (Case II) for ocean surveillance shows trends in system requirements as functions of radar system and operational parameters. The parameters specifically analyzed were: operating frequency, pulse length, swath width, azimuthal beamwidth, orbital altitude, antenna size, average and peak power, elevation beamshaping, and swath position relative to different outer-bound grazing angles.

(S) In the development of the radar equation for the Case II analysis, consideration is given to: sea clutter models, tropospheric propagation losses, system losses, Faraday rotation effects, signal integration, and partial sea clutter integration effects.

PROBLEM STATUS

(S) This is an interim report on one of three basic types of radar systems under consideration for use in a satellite ocean surveillance program.

AUTHORIZATION

NRL Problem R02-46

Project A37538-006/6521/F019-02-01

CONTENTS

OCEAN SURVEILLANCE RADAR PARAMETRIC ANALYSIS
CASE II - NON-COHERENT SIDELOOKING RADAR
(Unclassified Title)

Background (S) The Aerospace Radar Branch has been working on an AirTask for the study and development of a radar sensor for a Satellite Ocean Surveillance Program. As an initial part of that program, the Branch is engaged in the analysis of three basic types of systems: Case I, the non-coherent forward scan radar; Case II, the non-coherent sidelooking radar; and Case III, the coherent synthetic aperture sidelooking radar.

SIDELOOKING RADAR - CASE II

(S) The Case II radar is predicated on a simple, state-of-the-art, high reliability radar system. The antenna is potentially one of the simplest configurations considered for satellite ocean surveillance because neither mechanical nor electronic scan is required and it is not dependent upon the generation of a synthetic aperture. The sidelooking configuration uses a fixed antenna looking out to the side in a direction perpendicular to the orbital track of the satellite. Antenna scan is provided by the motion of the satellite. The fixed antenna may incorporate vertical beamshaping and a fixed down-tilt from the local horizon to provide optimum illumination of the required swath on the ocean surface. The geometry and coverage of the sidelooking antenna radar is shown in Fig. 1.

(U) A double sidelooking system is a natural development of the single sidelooking system, but tradeoffs and cost effectiveness of such evolutionary developments are to be considered in the final engineering analysis report.

OBJECTIVES

General (S) The objectives of the analysis program are to perform a parametric analysis of ocean surveillance radar systems with the aid of computer programs; to establish trends within given types of systems and to develop

realistic constraints and bounds; to evaluate, identify, and rank these systems on a cost effective basis. The first two of these objectives are covered in this report for the Case II radar system. In the subsequent study of systems cost effectiveness there will be a continued development and refinement of constraints and limits. Companion reports analyze the other two general systems types. A final engineering analysis report will be addressed to the cost effectiveness considerations of the several systems.

Operational (S) Lacking Specific Operational Requirements (SOR), the computer programs have as a required objective the detection of a non-fluctuating ship target with an effective radar cross-section of 200 square meters. Such a cross section is generally compatible with a small sea-going vessel of about 100 ft. in length when viewed bow or stern-on, or with the beam aspect of a surfaced submarine[1].

(U) Based on the probability of detection developed in reference (2), the probability of detection is required to be 0.99 per orbital scan of the antenna past the target, with an accompanying probability of false alarm of 1×10^{-10}. These conditions require an integrated signal-to-clutter + noise ratio of 16 dB at the output of the radar system data processor.

THE RADAR EQUATION - CASE II COMPUTER PROGRAM

(U) The following is intended to develop the radar equation, as found in numerous references, into the form used in the Case II radar analysis. Appendix A defines the terms and associated relationships in the Case II radar equation.

(U) The signal power returned from a target is[3]

$$S = \frac{P_t G^2 \lambda^2 \sigma_t}{(4\pi)^3 R_s^4} \qquad (1)$$

where S = received signal power

P_t = equivalent peak power

G = antenna power gain

λ = wavelength

σ_t = target radar cross-section

R_s = slant range to target

(U) It is assumed that the same antenna is used for transmitting and receiving and that a consistent set of units is used throughout. The following is the relationship[4] between the equivalent peak power (P_t) and the average transmitted power (P_{AV}) for a pulse compression system.

$$P_t = \frac{P_{AV}}{\tau_c \, (PRF)} \tag{2}$$

where τ_c = compressed pulse length

(PRF) = pulse repetition frequency

(U) Equation (2) illustrates that numerous systems could be defined using different pulse lengths and peak powers that would satisfy the average power requirement. Therefore, substituting (2) in (1), the following is obtained:

$$S = \frac{P_{AV} G^2 \lambda^2 \sigma_t}{(4\pi)^3 R_s^4 \tau_c \, (PRF)} \tag{3}$$

(U) By this same procedure, the signal power (C) returned from clutter is:

$$C = \frac{P_{AV} G^2 \lambda^2 \sigma_c}{(4\pi)^3 \gamma_c (PRF) R_s^4} \quad (4)$$

where σ_c is the radar cross-section of sea clutter.

(U) The number of statistically independent sea clutter returns, n_c, is related[2] to the product of the decorrelation time (T_d) and the (PRF) by the following expression:

$$T_d (PRF) \leq 1 \text{ uncorrelated, use } n_c = n \quad (5a)$$

$$T_d (PRF) \geq 1 \text{ partial correlation, use } n_c = \frac{n}{T_d (PRF)} \quad (5b)$$

where n = the number of pulses within the 3 dB azimuth beamwidth

(U) The noise power (N) associated with the radar system is[3]:

$$N = k T_i B_n \quad (6)$$

where k = Boltzmann's constant

T_i = effective system noise temperature, Table IV

B_n = receiver noise bandwidth (reciprocal of τ_c)

(U) Using equations (3), (4), and (6), the signal-to-clutter + noise ratio $\left[\left(\frac{S}{C+N}\right)_1\right]$ for one pulse can be written as:

$$\left(\frac{S}{C+N}\right)_1 = \frac{\dfrac{P_{AV} G^2 \lambda^2 \sigma_t}{(4\pi)^3 \tau_c (PRF) R_s^4}}{\dfrac{P_{AV} G^2 \lambda^2 \sigma_c}{(4\pi)^3 \tau_c (PRF) R_s^4} + N_o B_n} \qquad (7)$$

where $N_o = k T_i$

(U) When n pulse returns are integrated, a new signal-to-clutter + noise ratio $\left[\left(\frac{S}{C+N}\right)_n\right]$ can be defined which reflects the improvement due to the integration[4].

$$\left(\frac{S}{C+N}\right)_n = \left(\frac{S}{C+N}\right)_1 S_i (n) \qquad (8)$$

where $\left(\frac{S}{C+N}\right)_n$ = signal-to-clutter + noise ratio when n pulses are integrated

$S_i (n)$ = integration-improvement factor when n independent pulses are integrated

(U) Using equation (8) in equation (7) and solving for P_{AV}:

$$P_{AV} = \frac{(4\pi)^3 \tau_c N_o B_n (PRF) R_s^4 \left(\frac{S}{C+N}\right)_n L_T}{G^2 \lambda^2 S_i(n) \left[\sigma_t - \sigma_c' \frac{\left(\frac{S}{C+N}\right)_n}{S_i(n_c)}\right]} \qquad (9)$$

where L_T = the total system losses

where the integration-improvement factor ($S_i(n_c)$) associated with the clutter term was modified according to equation (5).

Effects of Faraday Rotation[4] Are Considered.

(U) These effects are discussed in the sections on constraints and limitations. L_{FR} is defined as the loss due to Faraday rotation where the values for L_{FR} come from Table I, and is used as shown in equation (10).

(U) The increase in σ_c due to Faraday rotation is handled by the use of a coefficient (ζ) based on values from Table II and is used as shown in equation (10).

(U) The final form of the radar equation, as used in the Case II radar computer program is:

$$P_{AV} = \frac{(4\pi)^3 \tau_c N_o B_n (PRF) R_s^4 \left(\frac{S}{C+N}\right)_n L_T}{G^2 \lambda^2 L_{FR} S_i(n) \left[\sigma_t - \sigma_c \frac{\left(\frac{S}{C+N}\right)_n}{S_i(n_c)} \zeta\right]} \qquad (10)$$

CONSTRAINTS AND LIMITATIONS

(S) The constraints and limitations operating in the computer-aided analysis of the Case II radar systems are described in the sections which follow. It should be noted that when possible and practical, identical constraints and limits were applied in each of the three cases. The sea clutter model, the tropospheric loss model, and losses resulting from Faraday rotation are common to each of the cases while constraints on such parameters as antenna size and azimuthal resolution may not be common.

Sea Clutter Models (S) The sea clutter models are shown in Fig. 2 (see reference (2) for the development of these models). Curve A of Fig. 2 (L-band data) is used as the model for 140, 220, 440, 900 and 1300 MHz sea clutter values. Curve B (S-band data) is used for the 2900 MHz computations, and Curve C (X-band data) is used for the 5250 and 8500 MHz computations.

Rain Model (U) A rain model is being developed for use with the computer aided parametric analysis discussed in this report. As a consequence, rain attenuation effects are not included in this present analysis, but will be included in the continuing analysis program. Including the rain model in the computer program will probably reveal a negligible effect on frequencies below 3000 MHz, and increasingly severe effect on higher frequencies.

Tropospheric and Ionospheric Range Model (U) The present model for obtaining slant range, depression, and grazing angles is based on a straight line ray path approximation for the atmosphere. A refined model[5] based on the refractive phenomena of the troposphere and ionosphere is available and will be included in the continuing analysis program. The raytrace model will correct a 3.3 percent error in range at the lowest usable frequency and smallest grazing angle. In general, as the grazing angle and frequency increase, the effect on range becomes negligible.

Faraday Rotation (S) Faraday rotation effects are three-fold: first, there is an effective reduction in antenna gain resulting from the rotation of the received energy from the plane of the receiving antenna (see Table I); second,

there is an increase in the sea clutter return when the plane of the incident energy at the sea surface has been rotated so that the predominant component is vertically polarized (see Table II); and third, the rotation to a predominantly vertical polarization at the sea surface results in ship radar cross sections that average 4 dB less than can be achieved with horizontal polarization.

Tropospheric and System Losses (U) Table III shows the total system losses as developed in reference (2). The losses include the antenna pattern, system degradation, transmission line, and tropospheric losses. It is to be understood that certain of these losses are provisional and are dependent upon a further definition of system configurations.

Noise Figure and Effective System Input Noise Temperature (U) Table IV lists the noise figures and effective system input noise temperatures. The noise figures are to be regarded as conservative values and are representative of values achieved with present-day operational systems.

(U) The effective system input noise temperature developed in reference (2) includes cosmic, solar, tropospheric, and ground-noise contributions, together with the receiver noise figure and receiver transmission line losses. The system input noise temperature in Table IV is developed for two grazing angles. Figure 3 is a plot for these two grazing angles which shows that the temperature minimizes at about 550 MHz. The 10-degree grazing angle values were used in the computer program as representative of values in the 1 to 40-degree grazing angle region.

Frequency (S) The analysis has been restricted to 8 discrete frequencies selected from the 100 to 10,000 MHz range. The frequencies selected were judged to cover the maximum useful spectrum for military systems (Ref. (1)) and represent a sampling sufficient to allow the establishment of parametric trends. It is to be understood that a finer grained examination of frequencies will be carried out to verify the designation of an optimum frequency.

Pulse Length (S) Three pulse lengths are considered in the analysis. They are: 0.05 microseconds (approximately 25 ft), 0.10 microseconds (approximately 50 feet), and 0.20 microseconds (approximately 100 ft.). Shorter pulse lengths were not included because of the increasing difficulty of achieving wide-band, high-power output at the UHF end of the spectrum. Longer pulse lengths were not included because of the degradation of range resolutions together with the increasing competition of sea clutter with the ship targets.

Swath Widths (S) Swath widths were arbitrarily chosen at 200, 400, 600, 800, 1000, and 1200 nautical miles (n.m.). The swath width referred to in this report is a receiver range-gated swath; when antenna size constraints are in effect the gated swath does not coincide with the 3 dB reference level of the antenna's vertical beam pattern. The number and order of swaths was judged sufficient to permit the development of system trends as a function of range swath. Tradeoffs in subsequent cost effectiveness analysis will consider swath widths versus altitudes and percent of ocean surface coverage.

Orbital Altitude (S) Orbital altitudes considered in the analysis are 200, 400, 600, 800, and 1000 n. m. The 200 n.m. lower limit was set because of increasing orbital decay effects and the consequent requirement for altitude sustaining power. The upper limit was set because of concern over the satellite entry into the lower Van-Allen radiation belt and the increasing risk to the 1-year survival of solid-state components.

Azimuthal Beamwidth (S) In the computer program, values of 0.25°, 0.50°, 1.0° and 2.0° were selected as the azimuthal beamwidths. The lower limit of 0.25° was set by a $\lambda/16$ wavelength dimensional tolerance for the antenna (see reference (2)). The intermediate and upper beamwidth values are incremental changes employed to reveal system trends.

Antenna Size (S) The limits on packaging size and the extremes of height-to-length ratios for antennas to be erected in space are not completely known. However, for shrouds of a size that could be adapted to a Titan III-C launch vehicle, antenna cross-sections of 22,000 square feet have been deemed feasible by representatives of the aerospace industry.

(S) In this analysis a limit of 15,000 square feet and a maximum length of 500 feet have been set as constraints on antenna size. The computer program is arranged so that when the cross-section limit is exceeded, the 15,000 square foot area is assigned for the remainder of that computation. The length is maintained as specified by the azimuthal beamwidth, and a new non-optimum value of antenna height is determined. In turn, new values of gain and output power are computed for a constrained antenna. On the application of these constraints there will be a departure from the matching of the 3 dB elevation beamwidth with the specified range swath, and the 3 dB elevation beamwidth covers greater ranges than are included in the receiver range gate interval. The objective of examining

systems with constrained antennas is to determine what additional practical solutions are available, and to subsequently compare them on a cost effectiveness basis for systems with and without constraints.

(S) A computer analysis will also be prepared for an Atlas type launch vehicle. The Atlas will result in a payload-volume limited aperture of 5,675 square feet, compared to 22,000 square feet for a Titan III-C. The results of the computer analysis of the Atlas payload systems will be included in the final engineering analysis.

Average Power (S) At an early point in the analysis program, both average and peak power values were judged to be limiting factors relative to any practical satellite borne system. However, for the sake of examining trends an initial average power level of 10,000 watts was established. As the analysis developed, average powers were reduced successively to maximum allowable levels of 2000, and then 1000 watts.

COMPUTER DATA

(S) Table V is a reproduction of a single page of computer output for the Case II systems. The fixed parameters for this one set of computations are shown at the top of the Table and are: 200 n.m. range (swath width); 0.25° azimuthal beamwidth, 200 square meter non-fluctuating ship target; 0.050 microsecond pulse length (equivalent to approximately 25 ft. range resolution); and 0.65 θ_E where θ_E is the elevation beamwidth and 0.65 is a factor accounting for the degree of elevation beamshaping.

(S) The first column of data printout is the average power required for detection of the specified target with a 16.0 dB integrated signal-to-clutter + noise ratio. The "NEAR" and "FAR" designators indicate power required at the inner and outer edges of the swath respectively. The dual computation is required because the combination of swath width, swath position relative to the 0 degree grazing angle, the clutter model, and the vertical beamshaping factor result in conditions where the overall system power requirement may be set by the far range. At other times, because of constraints, the required power may be set by the near edge of the swath.

(S) The peak power tabulation is based on a 100:1 pulse compression ratio and serves the purpose of helping to identify the magnitude of the problem in selecting r-f power amplifiers for potential systems. The 100:1 is a conservative value and does not represent an upper limit on achievable pulse compression. Chirp-type pulse compression systems have been built with ratios of 300:1, and the combination of chirp together with other coding may permit the realization of compression ratios of greater than 1000:1.

(U) The number of pulses integrated is a function of the number of pulses within the 3 dB azimuth beamwidth of the antenna. The integration period associated with the inner swath bound could be a system limit, but for processors that allow for the integration period to vary as a function of range, the integration period could be optimized at all ranges within the swath bounds. The present analysis is based on a variable integration period.

(U) The PRF is the maximum pulse repetition frequency for unambiguous detection within the specified swath.

(S) The slant ranges are the ranges from the satellite to the inner and outer edges of the swath, measured in nautical miles.

(S) The frequencies used in the computer program are: 140, 220, 440, 900, 1300, 2900, 5250, and 8500 MHz. As a result of the several constraints applied to the computer program (antenna size, average output power, and Faraday rotation) there are no printed outputs for frequencies less than 900 MHz. Earlier computer runs with higher allowed average powers and zero Faraday rotation did result in data outputs for the lower frequencies.

(U) The grazing angle (ϕ) column indicates the grazing angle measured at the inner and outer bounds of the swath, on the ocean surface. (See Fig. 1).

(S) The tabular listing of depression angles (ψ) are measures of angles at the satellite of ray paths to the surface range swath boundaries. The difference between the two values "NEAR" and "FAR" is the elevation beamwidth at the satellite. (See Fig. 1).

(U) The antenna gain is the gain computed for the outer and inner edges of the specified swath.

(S) The antenna dimensions are given in feet. The antenna area in the first system is 66,621 square feet. This, however, is a computed value before testing for the 15,000 square foot limit on antenna area. In this case the area exceeded the limit. Application of the antenna area limit results in a recomputed height of 47.66 feet. Additional limits applied are the $\lambda/16$ dimensional tolerances which correspond to a maximum of 0.25° beamwidth in either azimuth or elevation.

(S) The altitude column is the orbital altitude in nautical miles. The computer was programmed to cover the range of 200 to 1000 n. m. in 200 n. m. increments.

(U) The last column shown in Table V is the system loss associated with the two-way paths to the outer and inner bounds.

TRENDS

(U) The average power has been selected as the primary reference in the parametric analysis for the establishment of trends.

Frequency (S) The general trend of average power versus frequency is shown in Fig. 4. The parameters maintained as constants in these plots are: Pulse length, swath width, azimuth beamwidth, grazing angle, and the vertical beam-shaping factor. The additional parameter varied to form a family of plots is the orbital altitude.

(S) The plot of the 200 n. m. altitude data illustrates the influence of the several constraints on particular solutions of the radar equation. From 8500 to 2900 MHz the average power required varies as a logarithmic function of frequency. An extension of the line A-B to point C is an approximate indication of solutions that would be anticipated with the removal of antenna size constraints. It is an approximation because the magnitude of Faraday rotation effects have not been computed for this region, and it will be examined in more detail in subsequent computer runs and analyses.

(S) The segment D-E and its extrapolation to C, represent solutions for the same 200 n. m. altitude system, but with the condition that the antenna is constrained to 15,000 square feet in size.

(S) The additional plots for the higher altitudes show the same general trends of increasing power for increasing frequency when the antenna size is less than the 15,000 square foot limit. A second trend of interest is the power required as a function of altitude. Comparison of the several plots reveals that the power requirement increases with altitude up to 600 n. m. At 800 and 1000 n. m. altitudes, powers in the unconstrained regions (above 2900 MHz) are less than those for 600 n. m. The reason for the 600 n. m. altitude being the worst case is an apparent result of shaping of the vertical beam of the antenna. In the event of the specification of different swaths or the use of different beamshaping factors, a different worst case altitude would result. Further examples of this type will be discussed in the section on beamshaping.

Pulse Length (S) In Fig. 5 two families of plots show the comparative insensitivity of required average power as a function of pulse length. The two plots show that with other factors being held constant, greater power is required for the steeper grazing angles. At shallow grazing angles with a noise limited system, pulse length has comparatively little effect on the required average power. At steeper grazing angles, a clutter limited situation exists and power required increases markedly with increasing pulse lengths. As an example: At 2900 MHz and a 4 degree grazing angle, increasing the pulse length from 0.05 to 0.20 microseconds requires a power increase of 23.4 percent, while at 2900 MHz and an 8 degree grazing angle, an identical change in the pulse length requires an increase in power of 40.0 percent.

Swath Width (S) The consequences of varying the range swath dimension are shown in Fig. 6. In this figure, the effects of Faraday rotation and the constraints on antenna size are the same as those discussed in the earlier section on frequency. In general, as is shown in Fig. 6, the larger the swath the greater the power required. A specific example will illustrate the dependence:

200 nautical mile swath

200 n. m. altitude
1-degree grazing angle at outer bound
0.05 microsecond pulse length
0.25 degree azimuth beamwidth
5250 MHz, frequency
53.95 ft. antenna length
36.28 ft. antenna height
50.82 dB, antenna gain
113.2 watts, average power required

400 nautical mile swath *

200 n. m. altitude
1-degree grazing angle
0.05 microsecond pulse length
0.25 degree azimuth beamwidth
5250 Mhz, frequency
53.95 ft. antenna length
8.80 ft. antenna height *
44.7 dB, antenna gain *
988 watts, average power required *

(S) The * denotes required modifications of the 200 n. m. swath system parameters to obtain the 400 n. m. swath. The antenna aperture has been decreased to provide the increased swath. This in turn, results in about 6 dB less gain. The decreased antenna gain plus the increased power required to compensate for the increased sea clutter results in a power increase of over 9 dB. (113.2 to 988 watts).

Altitude (S) Figures 4, 7 and 8 show the influence of altitude on the average power. In Fig. 4, trends are shown for a small range swath of 200 n. m. These trends were discussed in the earlier section on frequency.

(S) In Fig. 7, data on a 400 n. m. swath is presented. With the larger swath, increased power is required with increased satellite altitude. Further, the elevation beamshaping factor which is the same as that used in Fig. 4, now represents a better fit of the elevation beam pattern to the range swath. As a consequence, a critical or worst case altitude is not developed as was noted for the 600 n. m. example in Fig. 4.

(U) In Fig. 8, a different aspect of the altitude and power relationship is developed. The frequency is fixed while the outer grazing angle boundaries are varied to generate a series of plots.

(S) Again there is evidence of the general trend that increased satellite altitude requires increased average power output. Exceptions in the general trend are evidenced in parts of the 6 and 8 degree plots. Elevation beamshaping, which is discussed later, causes a departure from the general trend.

Outer Grazing Angle Boundary (S) Fig. 9 shows the influence of the position of the swath on the power requirements. The plots shown in Fig. 9 are for a 200 n. m. altitude and a 400 n. m. swath. The plots show that if the swath width is maintained constant but brought closer to the satellite ground track, the average power required increases. The reasons for increased power are: As the grazing angles get steeper the clutter level increases; and to maintain the same swath at steeper grazing angles requires that the elevation beamwidth be increased. This in turn requires a reduced antenna height which results in a lowe antenna gain and a higher average power.

Azimuth Beamwidth (S) Power as a function of frequency and azimuth beamwidth is shown in Fig. 10. It can be seen that as the azimuth beamwidth is increased, with other parameters held constant, the power increases.

Antenna Size (S) In Fig. 11 the curve for power versus frequency is identical with that for the 200 n. m. altitude plot on Fig. 4. The second plot is of the antenna cross section versus frequency for the identical set of computer data. This plot shows the inverse relationship between cross section and frequency. The discontinuous logarithmic plots are a result of the Faraday rotation effects and the antenna constraints.

Elevation Beamshaping (S) Figs. 12 and 13 illustrate the effect of the beamshaping factor on the solutions available for the Case II systems. This factor is one which modifies a $(\sin x)/x$ pattern with varying degrees of a $(\csc^2 x)(\cos x)$ function (See Appendix A for additional details). In Fig. 12, for the case of narrowest swath (200 n. m.), it is evident that shaping imposes a penalty and requires more power as the degree of vertical beamshaping is increased. Note: The factors 0.9, 0.8, 0.7, etc. represent increasing amounts of beamshaping where a factor of 1.0 indicates no shaping.

(S) In Fig. 13, the swath width is doubled to a value of 400 n. m., with the other parameters the same as in Fig. 12. For an increased swath, it no longer follows that in all cases the vertical beamshaping imposes a penalty. For this particular geometry the most effective illumination is obtained with a 0.65 shaping factor. Thus, optimized solutions can be achieved through an iterative adjustment of the degree of vertical beamshaping and the positioning of the beam center within the swath.

Future Program (S) The continuing parametric analysis is to be developed through the performance of the following tasks:

(a) Additional computer runs are to be made which incorporate the rain attenuation model and a ray path model which includes both tropospheric and ionospheric effects.

(b) A further analysis is to be made of vertical beamshaping and vertical beampointing effects.

(c) A separate analysis will be made of systems which can be launched with an Atlas vehicle.

(d) A cost effectiveness analysis is to be performed to determine the parameters for an optimum noncoherent sidelooking radar.

(e) The noncoherent sidelooking radar is to be compared on a cost effectiveness basis with the other major types of systems included in the parametric analysis program.

SUMMARY

(S) In this analysis of a noncoherent sidelooking radar for satellite ocean surveillance, the following constraints and limits have been developed:

(a) The satellite platform is restricted to weights and volumes compatible with a Titan III-C type launch vehicle.

(b) The antenna has been limited to a maximum length of 500 feet, a total cross section of 15,000 square feet, and a dimensional tolerance of $\lambda/16$.

(c) The average power output from the radar is limited to 1000 watts.

(d) For the detection of a non-fluctuating target with a 0.99 probability of detection and a 1×10^{-10} probability of false alarm, a 16 dB integrated signal-to-clutter + noise ratio must be maintained.

(S) The major trends are:

(a) The combination of limits on power and antenna size, together with the influence of Faraday rotation and sea clutter, effectively eliminate frequencies less than 900 MHz.

(b) The power required varies directly and linearly with frequency until the several constraining factors are encountered. In general, the range of optimum frequencies for the Case II systems is 1300 to 2900 MHz.

(c) In this analysis, pulse length has only a minor effect on the required average power. It should be based on trade-offs between desired range resolution, achievable power-amplifier bandwidths, and data processor storage requirements.

(d) Increasing range swath requires increasing average power.

(e) As altitude is increased the average power required also increases.

(f) In general, the optimum power solution is obtained by setting the outer bound of the swath near the zero degree grazing angle.

(g) The optimum power solution is obtained by choice of the narrowest permissible azimuth beamwidths.

(h) Required antenna size varies inversely with the frequency and the power.

(i) The effect of vertical beamshaping and the locations of the main beam center can be complex. A general observation is that for narrow swaths optimum results are obtained without vertical beamshaping. As swaths are broadened, the optimum solutions are obtained with varying degrees of beamshaping.

REFERENCES

1. (U) Donald E. Kerr (editor), Propagation of Short Radio Waves, Massachusetts Institute of Technology Radiation Laboratory Series, Volume 13, Chapter 6, (1951). McGraw-Hill Book Co. Inc., N. Y.

2. (U) Robert E. Ellis, Ocean Surveillance Radar Parametric Analysis, NRL Memorandum Report 1862, March 1968. (Secret Report, Uncl. Title)

3. (U) David K. Barton, Radar System Analysis, (1964). Prentice-Hall Inc., N. J.

4. (U) Merrill I. Skolnik, Introduction to Radar Systems, (1962) McGraw-Hill Book Company, Inc., N. Y.

5. (U) Lamont V. Blake, Program Raytrace (Personal communication of January, 1968.

TABLE I

Effective Reduction In Antenna Gain Due To Faraday Rotation *

Frequency MHz	Satellite Altitude (n. m.) 200 Loss-dB	400 Loss-dB	600 Loss-dB	800 Loss-dB	1000 Loss-dB
140	-20	-20	-20	-20	-20
220	-20	-20	-20	-20	-20
440	-20	-20	-20	-20	-20
900	-4.68	-20	-20	-20	-20
1300	-0.91	-3.37	-3.89	-4.09	-4.09
2900	-0.03	-0.10	-0.15	-0.15	-0.15
5250	-0.01	-0.01	-0.01	-0.01	-0.01
8500	0	0	0	0	0

* L_{FR} in dB

TABLE II

Effective Increase In Sea Clutter Resulting From Faraday Rotation From Horizontal To Vertical Polarization*

Frequency MHz	Satellite Altitude (n. m.) 200 dB	400 dB	600 dB	800 dB	1000 dB
140	10	10	10	10	10
220	10	10	10	10	10
440	10	10	10	10	10
900	0	10	10	10	10
1300	0	0	0	0	0
2900	0	0	0	0	0
5250	0	0	0	0	0
8500	0	0	0	0	0

* ζ in dB

TABLE III

Total System Losses vs. Frequency and Grazing Angle

Grazing Angle, Degrees	Frequency MHz 140 Loss dB	220 Loss dB	440 Loss dB	900 Loss dB	1300 Loss dB	2900 Loss dB	5250 Loss dB	8500 Loss dB
0	6.16	6.59	7.74	9.11	9.28	10.27	10.80	11.70
2	6.01	6.26	6.85	7.51	7.68	8.07	8.30	8.70
4	5.94	6.14	6.53	6.96	7.13	7.43	7.61	8.00
6	5.90	6.08	6.41	6.79	6.93	7.17	7.34	7.55
8	5.85	6.03	6.31	6.66	6.78	7.03	7.20	7.33
10	5.80	6.01	6.26	6.54	6.64	6.87	7.03	7.18
12	5.80	5.99	6.24	6.52	6.62	6.84	7.00	7.13
15	5.80	5.89	6.21	6.46	6.56	6.80	6.96	7.10
20	5.80	5.89	6.17	6.41	6.51	6.72	6.89	7.03
40	5.80	5.89	6.04	6.32	6.40	6.61	6.75	6.86

TABLE IV

Receiver Noise Figure and Effective System Input Noise Temperature vs Frequency

Frequency MHz	Receiver Noise Figure dB	Effective System Input Noise Temperature °k, @ 10° Grazing Angle *
140	3.0	1773
220	3.1	1098
440	3.4	790
900	3.9	829
1300	4.3	936
2900	5.7	1430
5250	6.9	2009
8500	8.0	2727

* For an ocean surveillance satellite-borne radar.

TABLE V
Computer Data Output

SWATH WIDTH = 200 N.MI. BEAMWIDTH = 0.25 DEG, TARGET SIZE = 200 SQ.MTRS. PULSE WIDTH =0.050 MICROSEC

THETAE0=(0.65) THETAE

	AVG POWER	PEAK POWER	NO. PULSES INTEG.	PRF	SLANT RANGE	FREQ	GRAZING ANGLE	DEPRESS ANGLE	ANT. GAIN	ANT. LENGTH	ANT. WEIGHT	ALT.	ANT. AREA	SYSTEM LOSSES
	WATTS	KW		PPS	N.MI.	MHZ	DEGREES	DEGREES	DB	FEET	FEET	N.MI.	SQFT	DB
NEAR	11.6	27.0544	92	86	932	900	4.90	19.68	45.08	314.74	47.66	200	66621	6.88
FAR	30.9	71.8616	113	86	1131	900	1.00	19.11	45.08	314.74	47.66	200	66621	8.31
NEAR	9.5	20.6610	92	92	876	900	6.17	20.02	45.08	314.74	47.66	200	45587	6.78
FAR	22.2	48.3094	115	92	1076	900	2.00	19.18	45.08	314.74	47.66	200	45587	7.51
NEAR	6.4	12.2411	91	104	775	900	8.79	20.94	45.08	314.74	47.66	200	26109	6.61
FAR	14.8	28.3899	116	104	974	900	4.00	19.48	45.08	314.74	47.66	200	26109	6.96
NEAR	14.4	24.4886	91	118	686	900	11.56	22.20	42.47	314.74	47.66	200	17094	6.52
FAR	10.7	18.1981	119	118	884	900	6.00	19.97	45.08	314.74	47.66	200	17094	6.79
NEAR	26.4	39.3804	91	134	608	900	14.50	23.80	40.38	314.74	38.22	200	12030	6.47
FAR	12.4	18.5413	122	134	804	900	8.00	20.63	44.12	314.74	38.22	200	12030	6.66
NEAR	34.2	45.2487	91	151	540	900	17.63	25.75	39.06	314.74	28.18	200	8869	6.43
FAR	17.2	22.7380	125	151	734	900	10.00	21.46	42.80	314.74	28.18	200	8869	6.54
NEAR	42.0	49.1485	92	171	481	900	20.97	28.06	37.88	314.74	21.48	200	6762	6.41
FAR	23.1	26.9960	130	171	673	900	12.00	22.42	41.62	314.74	21.48	200	6762	6.52
NEAR	53.6	52.5356	93	204	408	900	26.41	32.17	36.31	314.74	14.99	200	4719	6.38
FAR	33.6	32.9180	136	204	596	900	15.00	24.10	40.06	314.74	14.99	200	4719	6.46
NEAR	2.7	6.3724	92	86	932	1300	4.90	19.68	48.28	217.90	68.84	200	31931	7.04
FAR	7.3	16.9781	113	86	1131	1300	1.00	19.11	48.28	217.90	68.84	200	31931	8.48
NEAR	2.8	6.0302	92	92	876	1300	6.17	20.02	47.80	217.90	68.84	200	21850	6.92
FAR	5.3	11.4145	115	92	1076	1300	2.00	19.18	48.28	217.90	68.84	200	21850	7.68
NEAR	11.9	22.9647	91	104	775	1300	8.79	20.94	43.75	217.90	57.43	200	12514	6.72
FAR	5.0	9.6354	116	104	974	1300	4.00	19.48	47.49	217.90	57.43	200	12514	7.13
NEAR	19.0	32.1194	91	118	686	1300	11.56	22.20	41.91	217.90	37.60	200	8193	6.62
FAR	8.4	14.2921	119	118	884	1300	6.00	19.97	45.65	217.90	37.60	200	8193	6.93
NEAR	26.6	39.6599	91	134	608	1300	14.50	23.80	40.38	217.90	26.46	200	5766	6.57
FAR	12.6	18.7949	122	134	804	1300	8.00	20.63	44.12	217.90	26.46	200	5766	6.78
NEAR	34.3	45.3992	91	151	540	1300	17.63	25.75	39.06	217.90	19.51	200	4251	6.53
FAR	17.3	22.9273	125	151	734	1300	10.00	21.46	42.80	217.90	19.51	200	4251	6.64
NEAR	42.0	49.1540	92	171	481	1300	20.97	28.06	37.88	217.90	14.87	200	3241	6.50
FAR	23.3	27.1972	130	171	673	1300	12.00	22.42	41.62	217.90	14.87	200	3241	6.62
NEAR	53.3	52.2607	93	204	408	1300	26.41	32.17	36.31	217.90	10.38	200	2262	6.47
FAR	33.8	33.1024	136	204	596	1300	15.00	24.10	40.06	217.90	10.38	200	2262	6.56

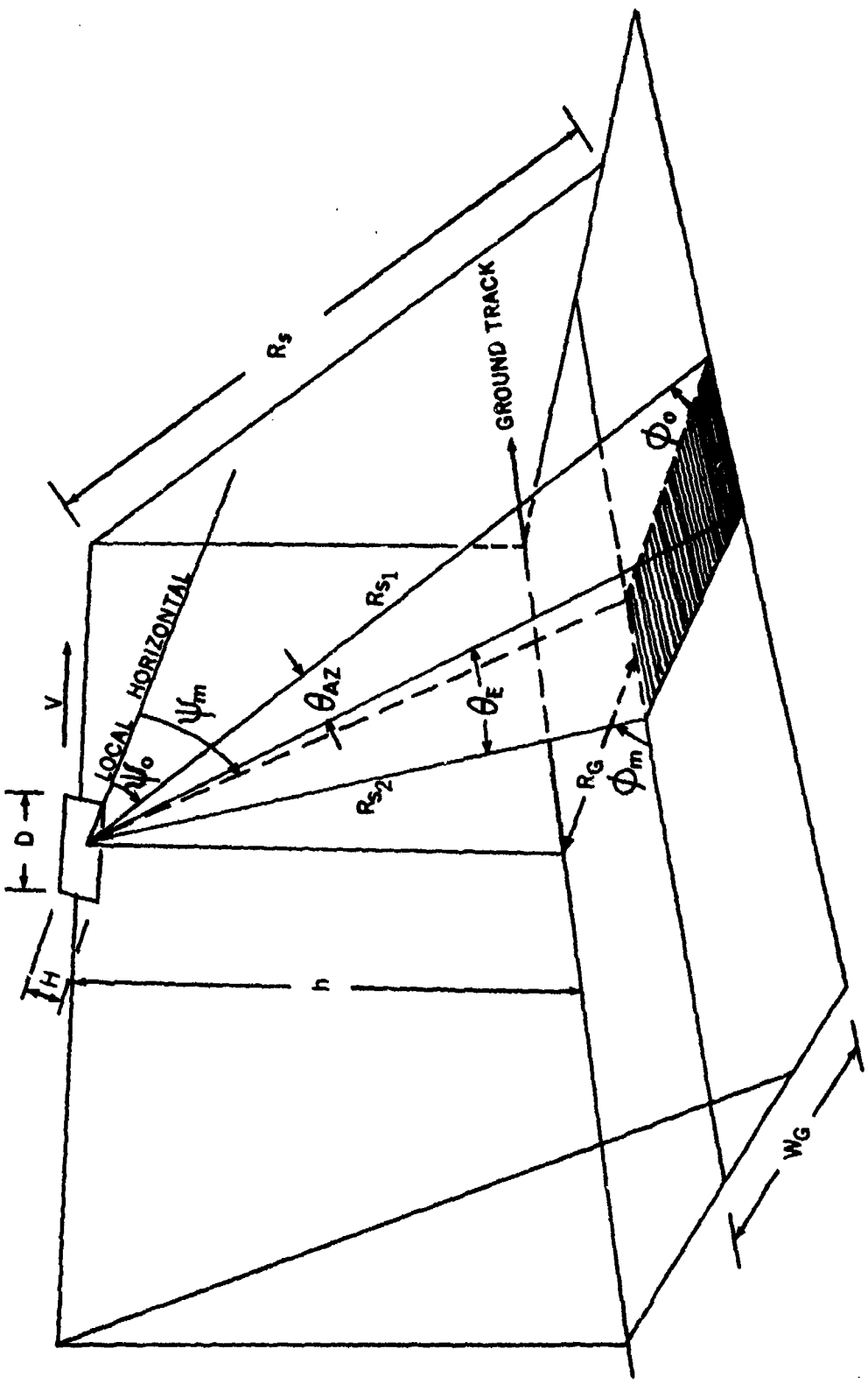

Fig. 1a - Sidelooking radar geometry

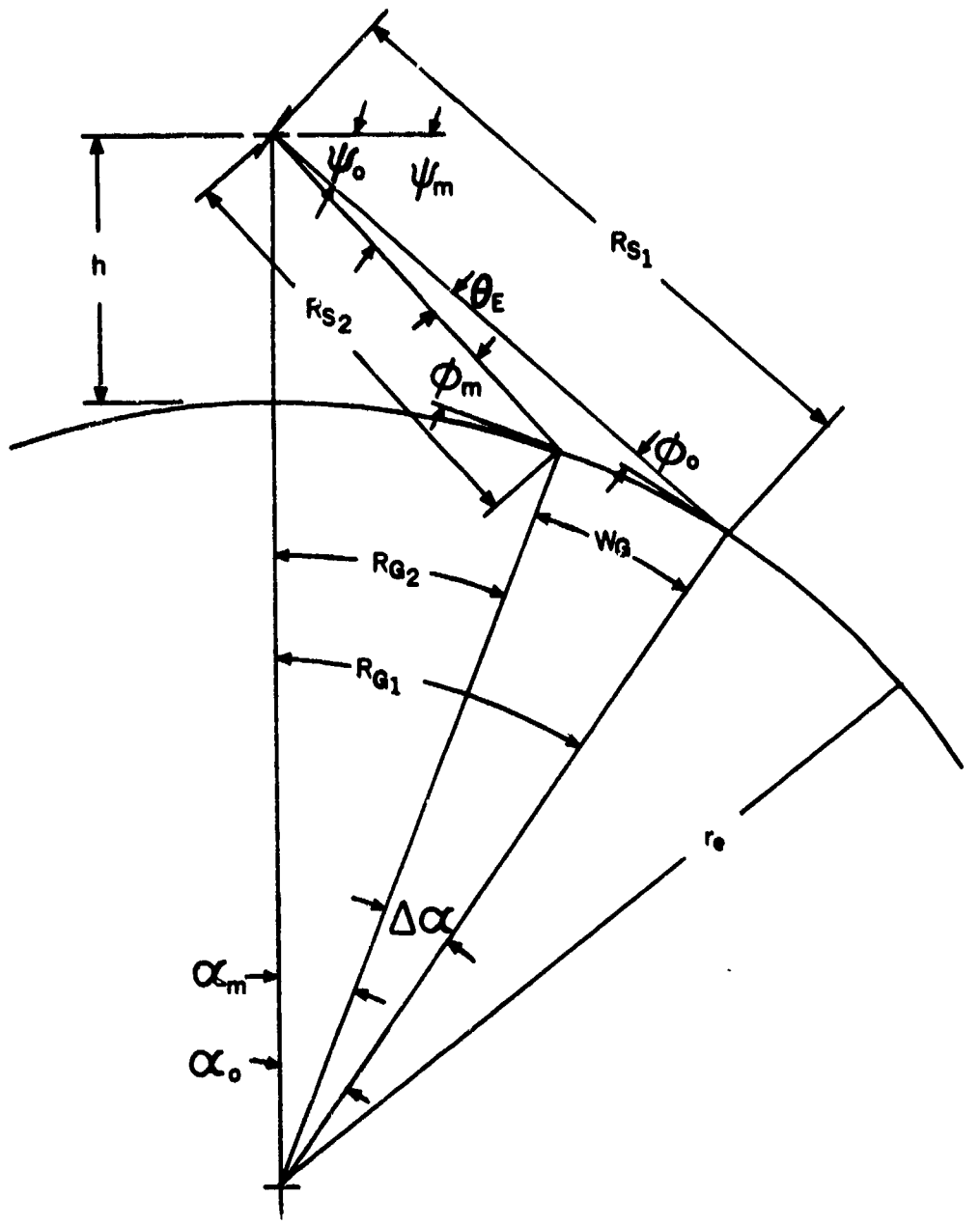

Fig. 1b - Sidelooking radar geometry

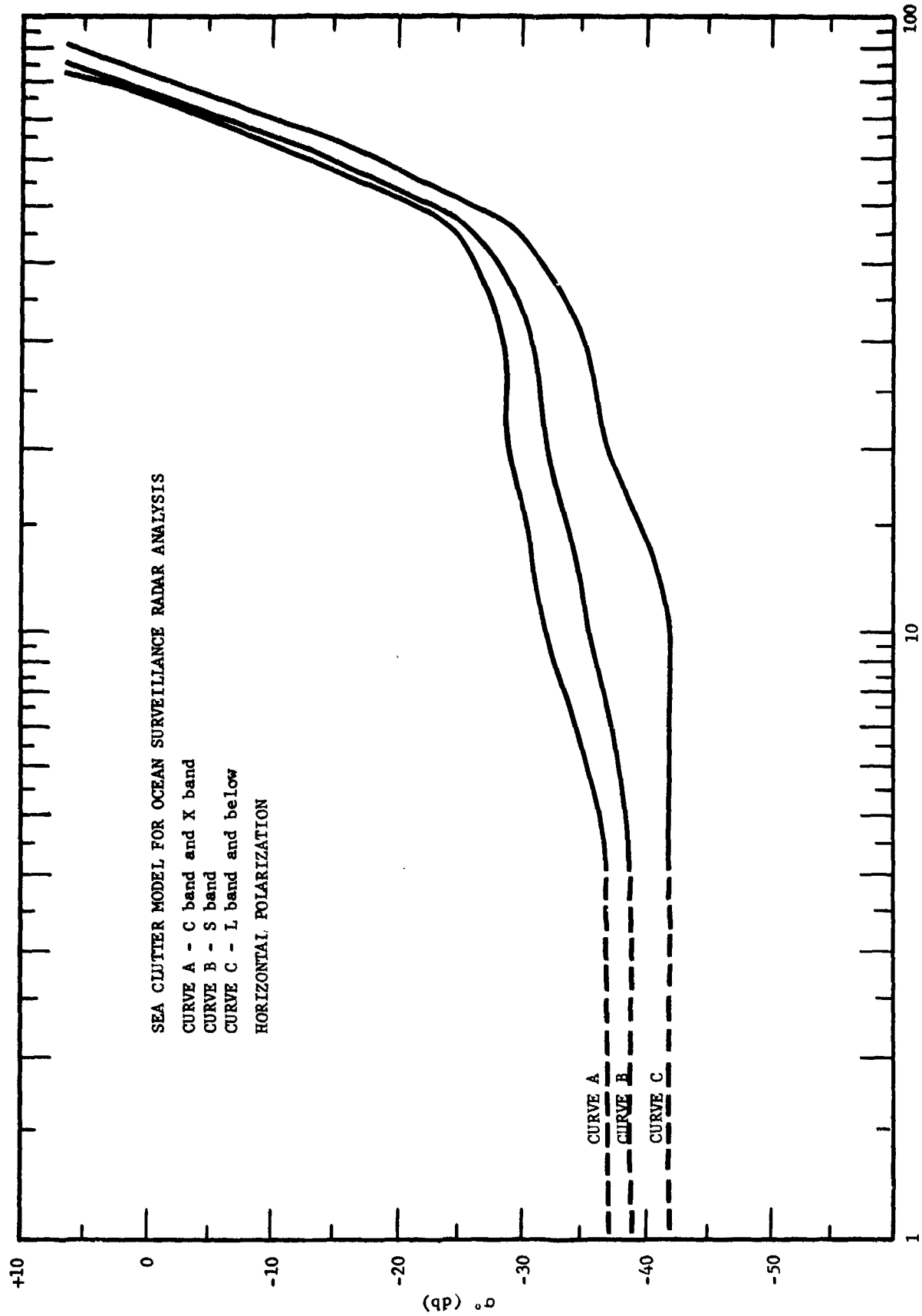

Fig. 2 - Sea clutter model for ocean surveillance radar

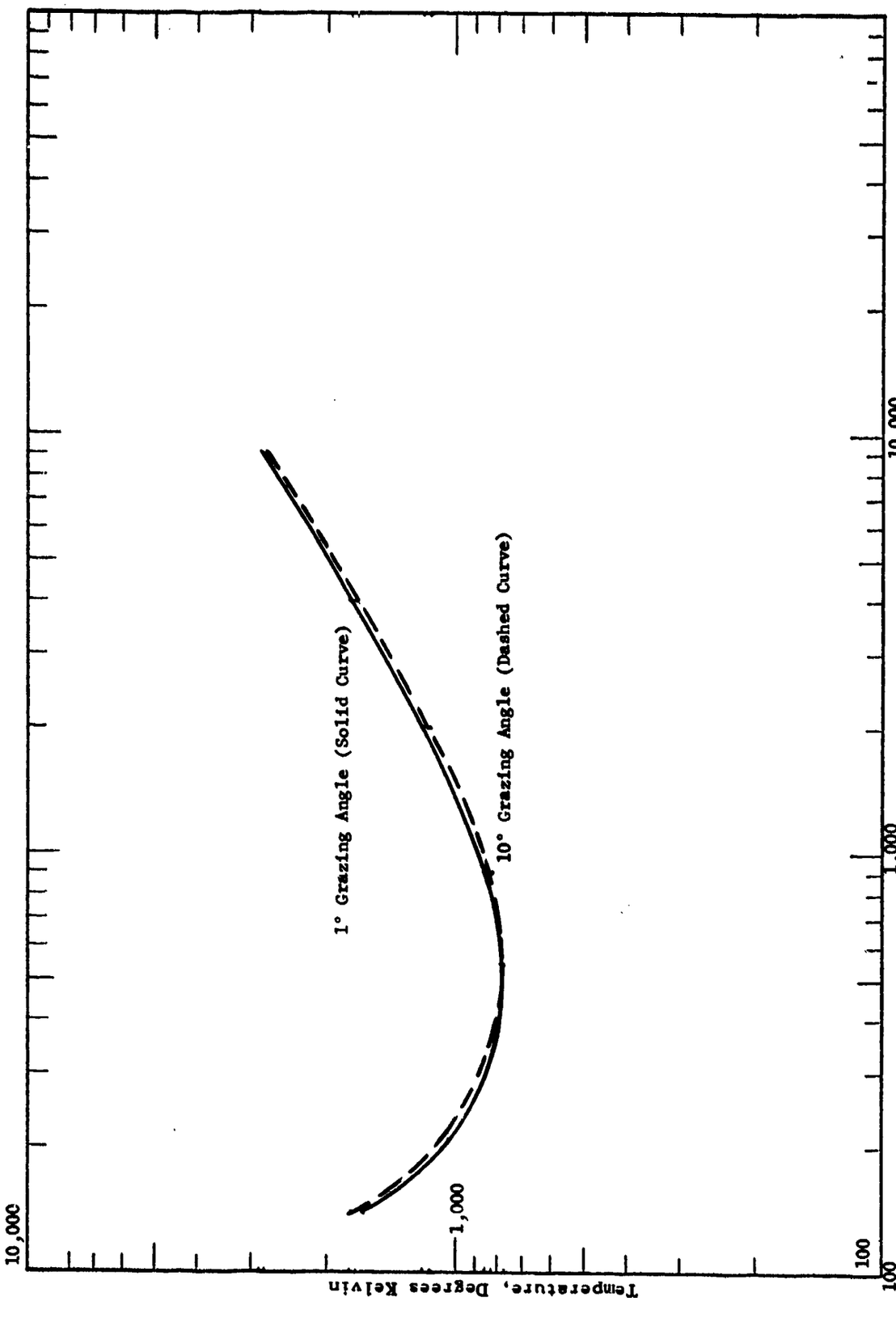

Fig. 3 - Effective system input noise temperature vs frequency

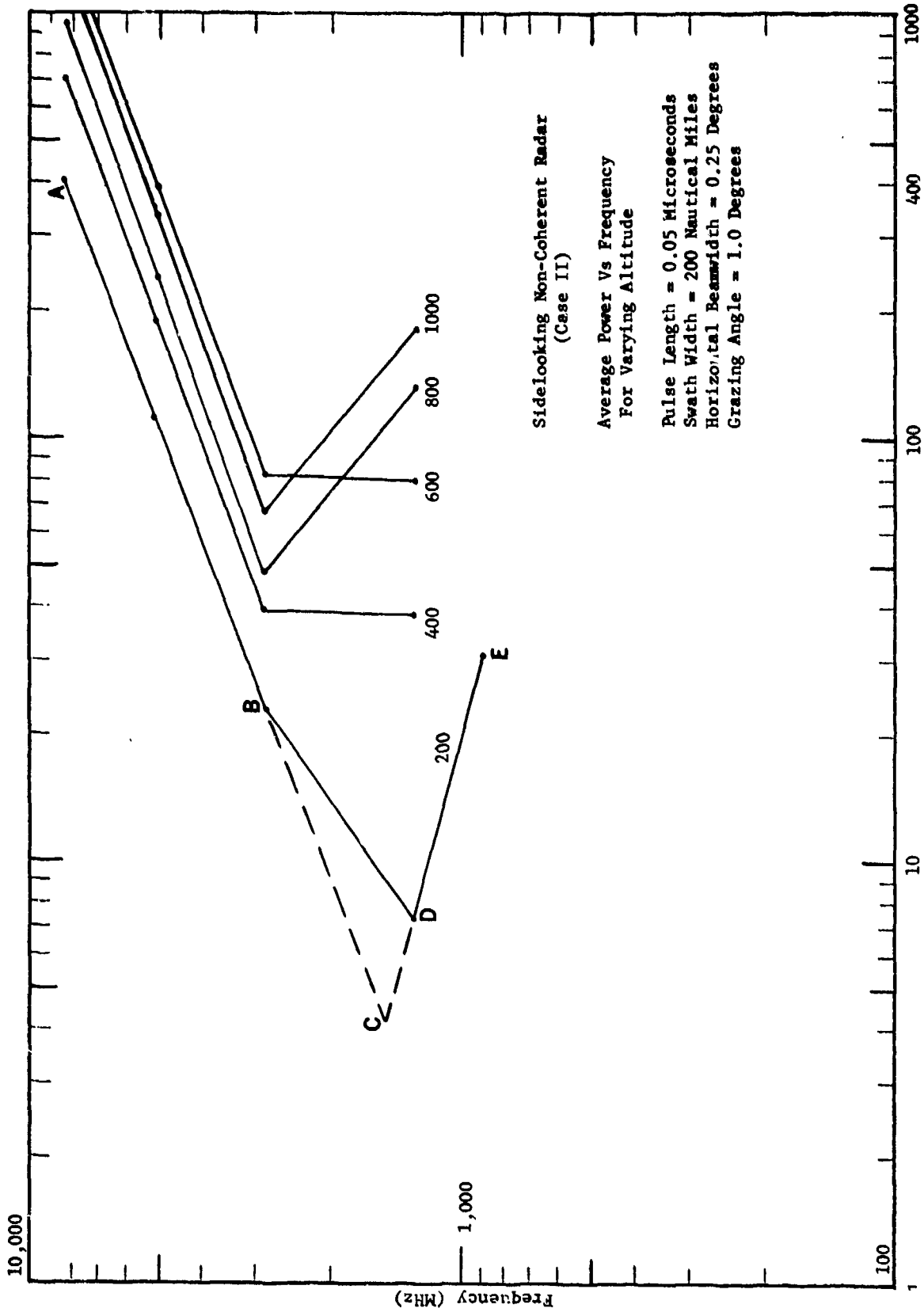

Fig. 4 - Average power vs frequency for varying altitude

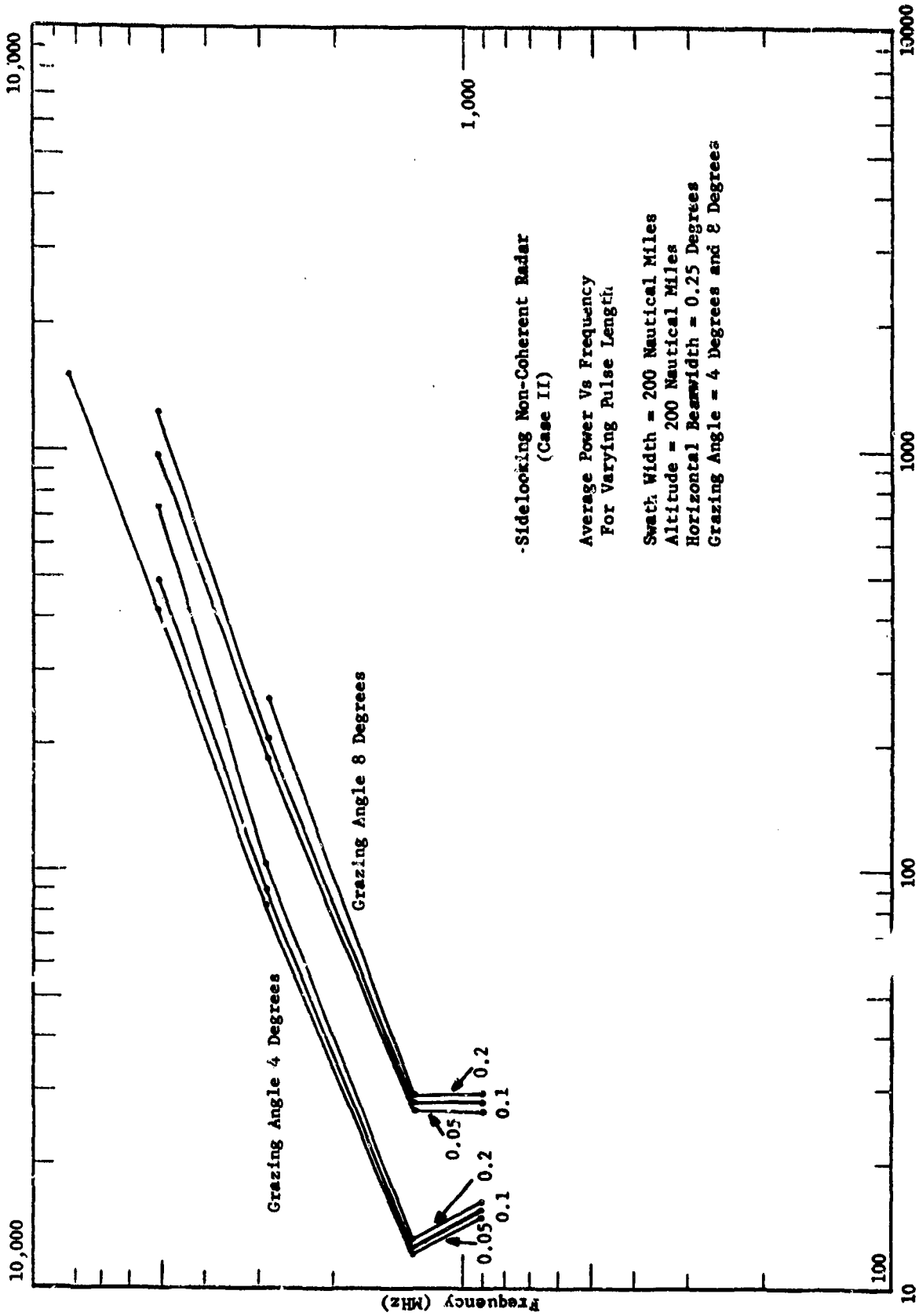

Fig. 5 - Average power vs frequency for varying pulse length

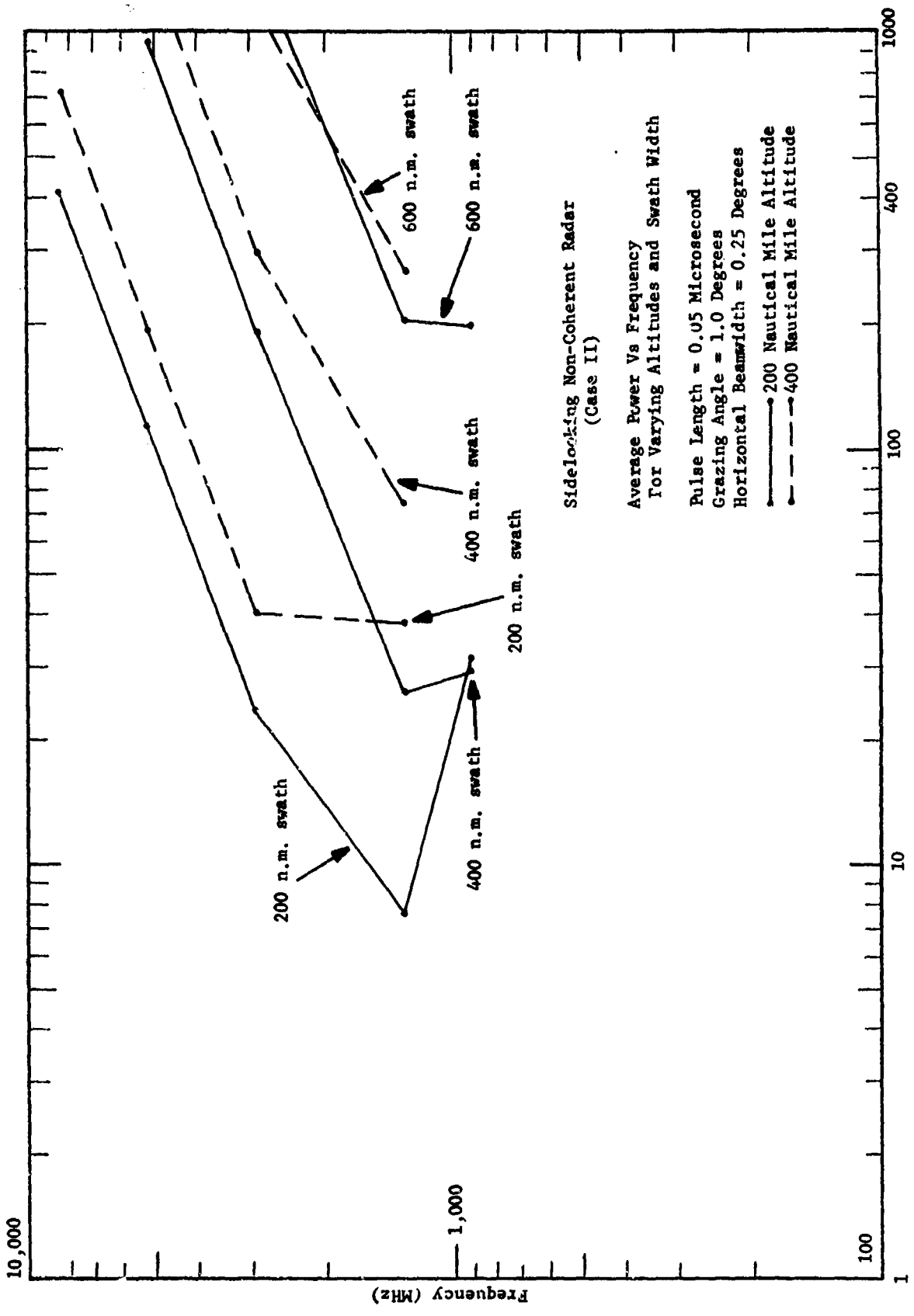

Fig. 6 - Average power vs frequency for varing altitudes and swath width

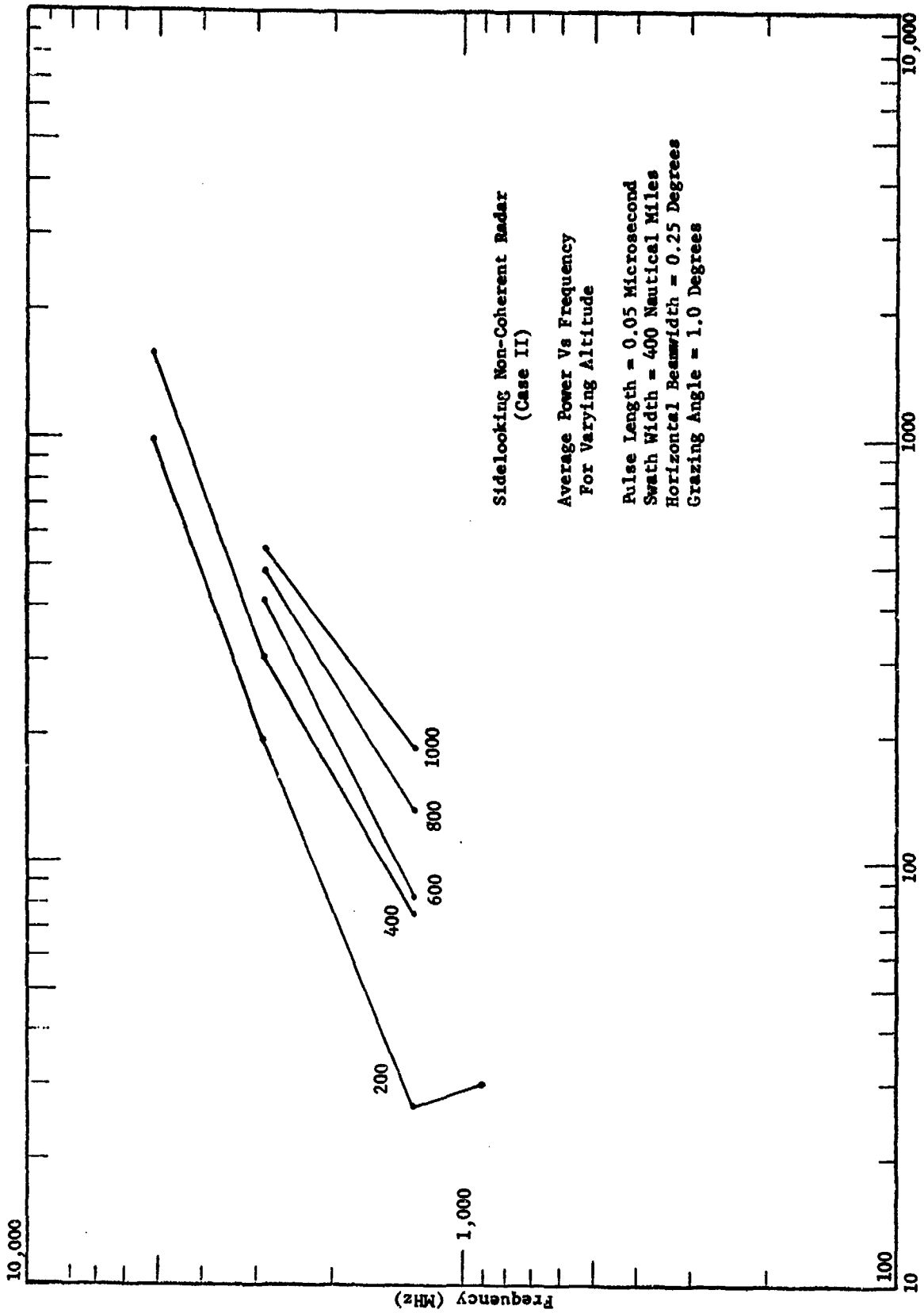

Fig. 7 - Average power vs frequency for varying altitude

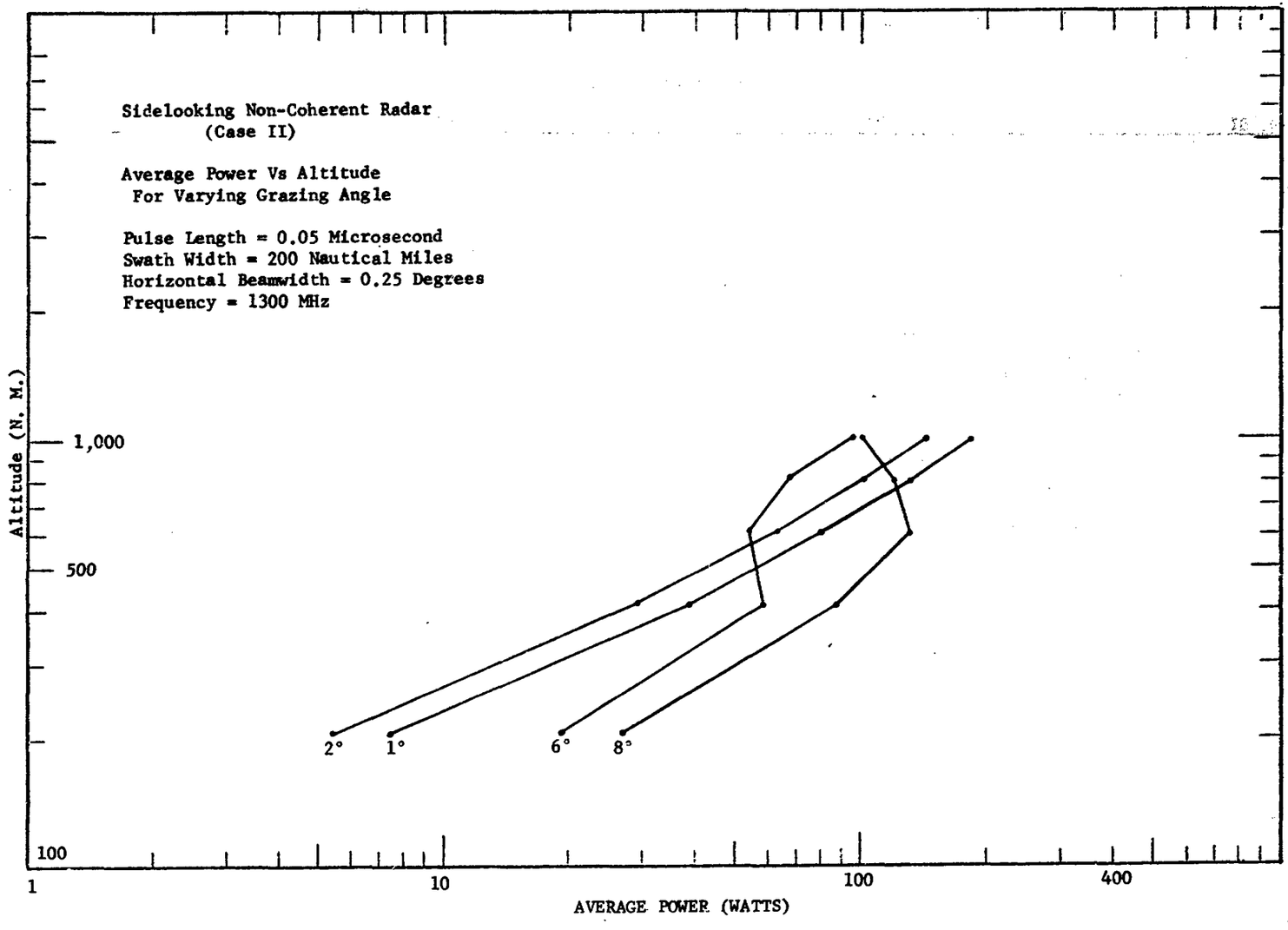

Fig. 8 - Average power vs altitude for varying grazing angle

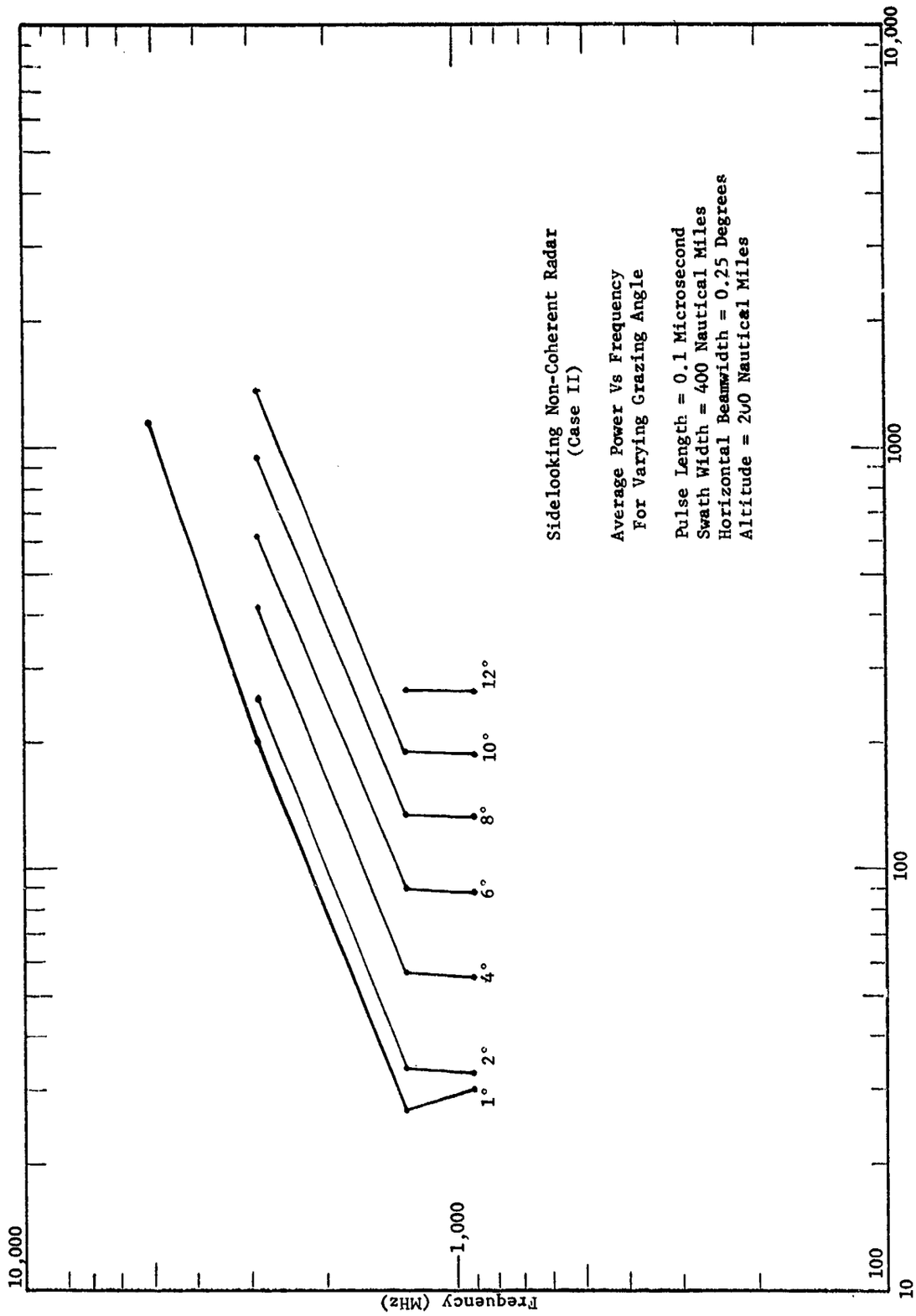

Fig. 9 - Average power vs frequency for varying grazing angle

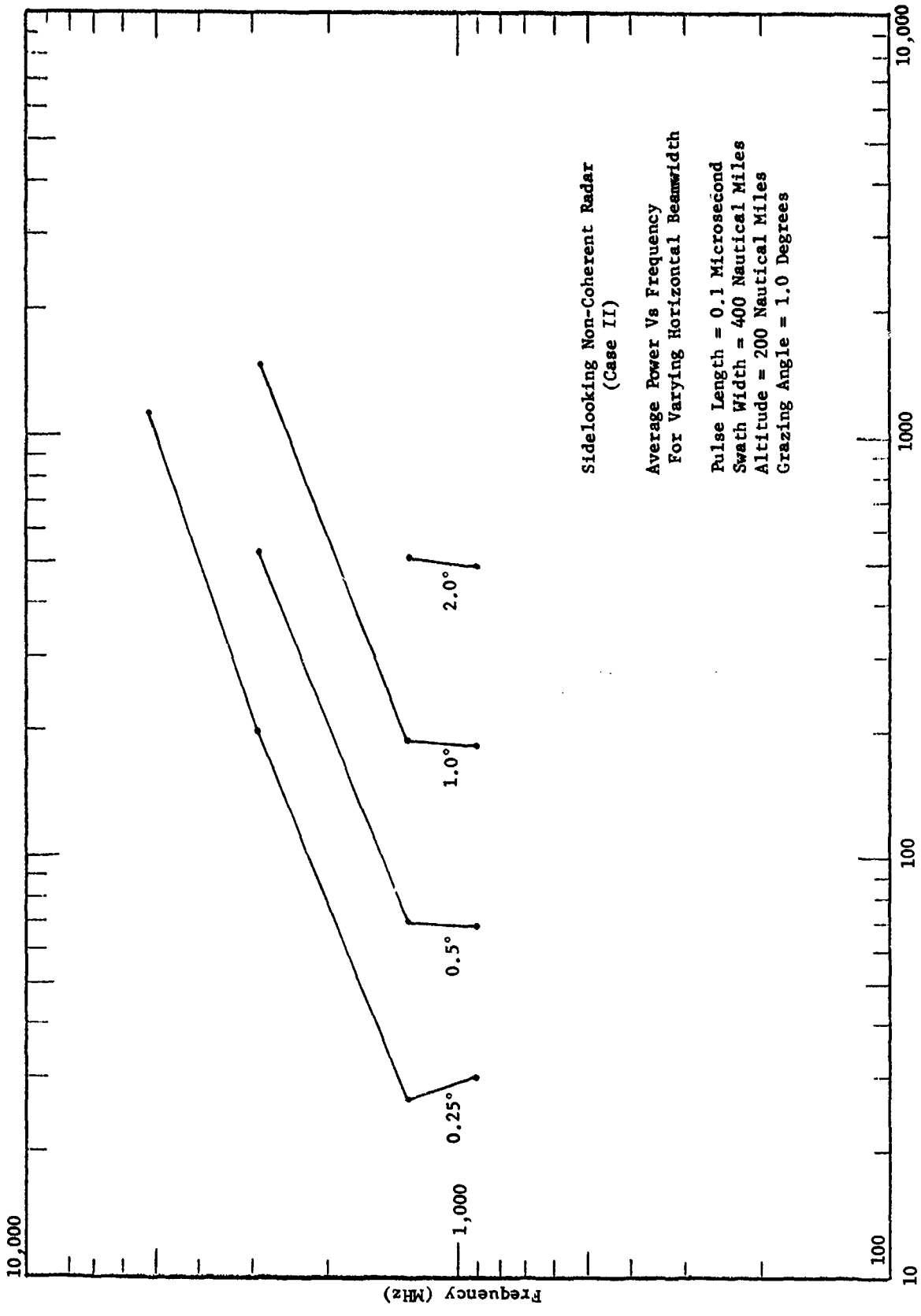

Fig. 10 - Average power vs frequency for varying horizontal beamwidth

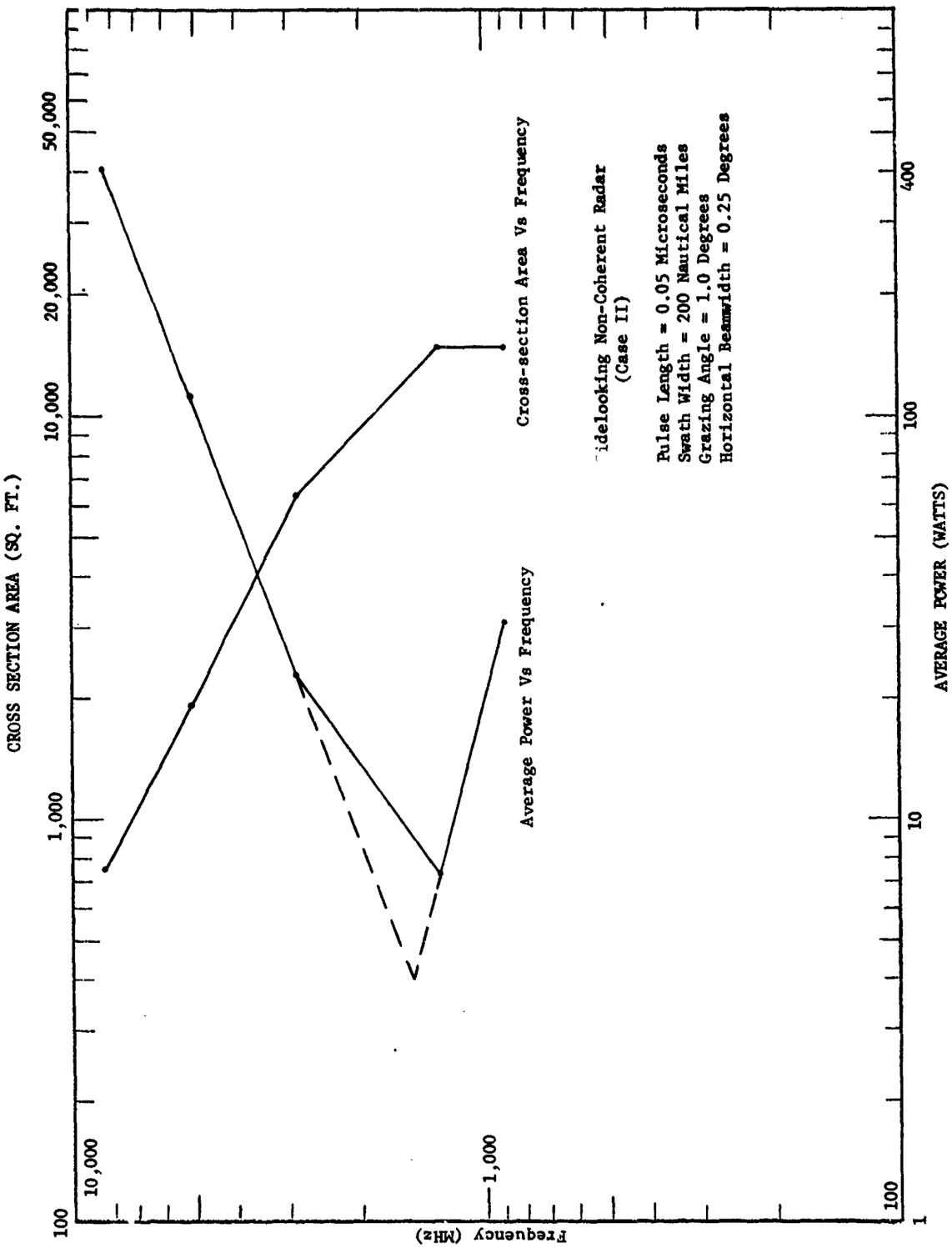

Fig. 11 - Average power vs frequency and antenna cross-section area

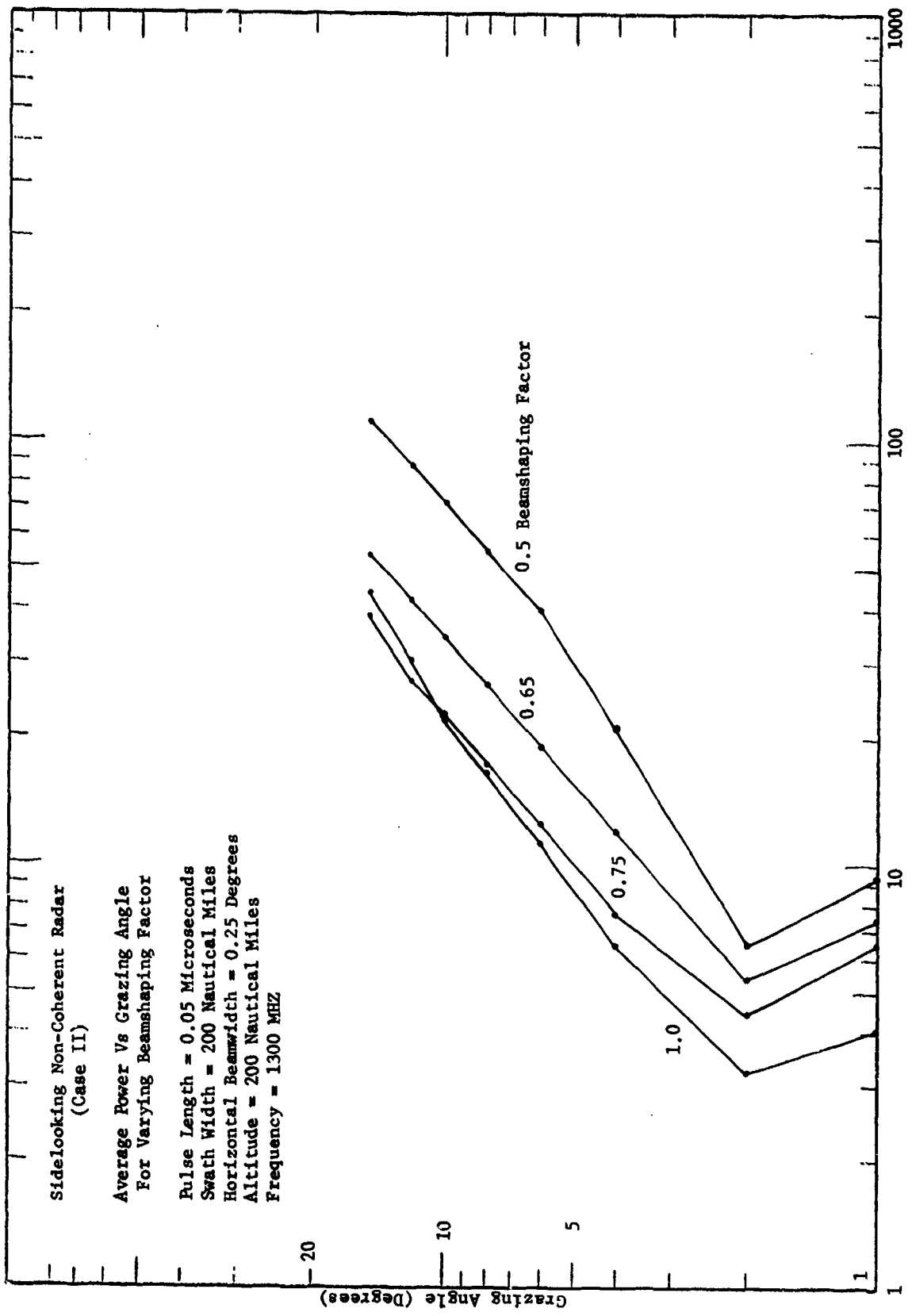

Fig. 12 - Average power vs grazing angle for varying beamshaping factor, 200 mile swath

(Page 38 is Blank)

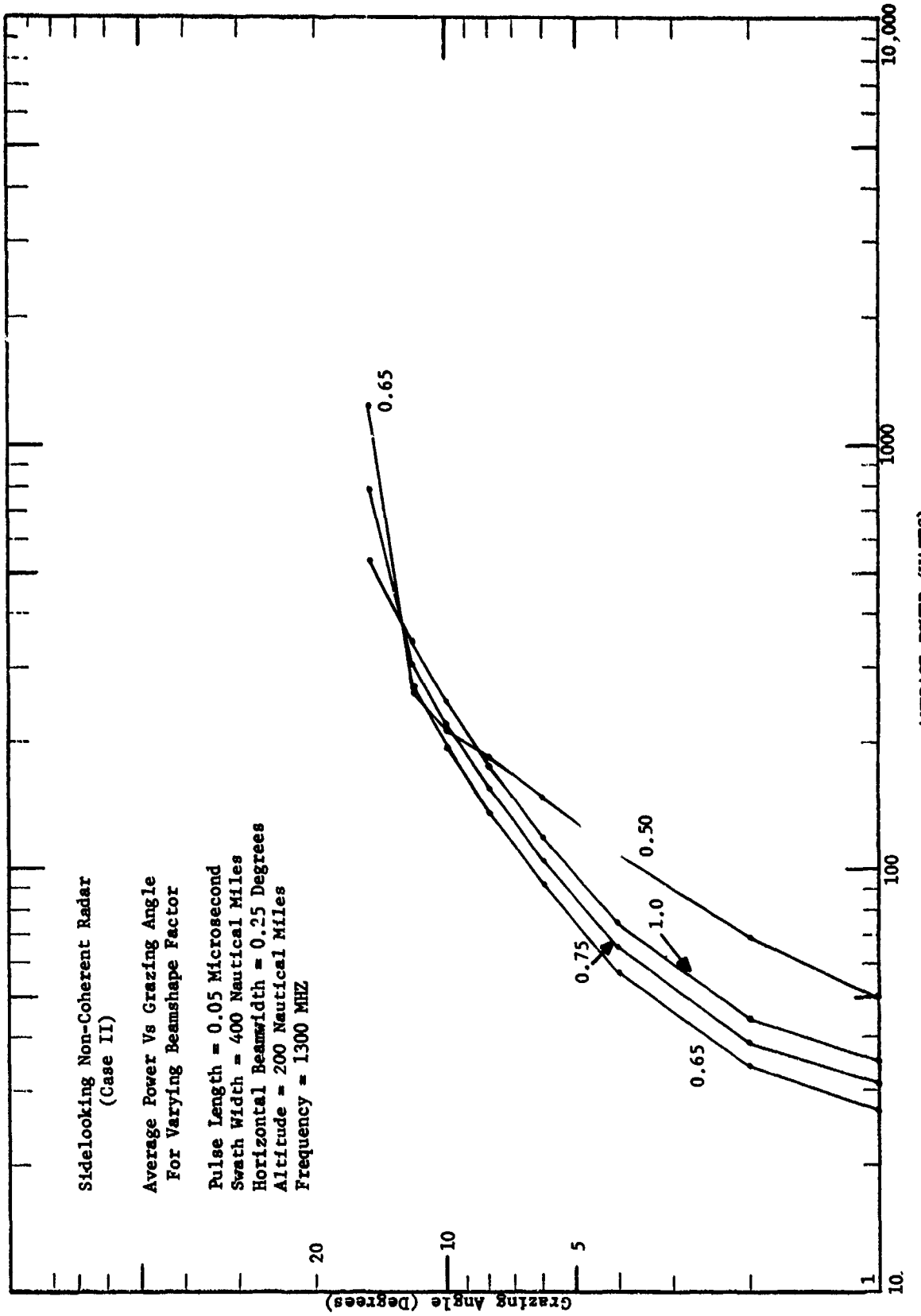

Fig. 13 - Average power vs grazing angle for varying beamshaping factor, 400 mile swath

APPENDIX A

DEFINITION OF UNITS AND ASSOCIATED RELATIONSHIPS FOR THE CASE II RADAR EQUATION

$$P_{AV} = \frac{K\ (4\pi)^3\ B_n\ \tau_c\ \left(\frac{S}{C+N}\right)_n\ L_T\ N_o\ R_s^4\ (PRF)}{G^2\ \lambda^2\ S_i\ (n)\ L_{FR}\ \left(\sigma_T - \sigma_c'\ \frac{\left(\frac{S}{C+N}\right)_n\ \zeta}{S_i\ (n_c)}\right)}\ , \text{watts} \qquad (1)$$

where:

P_{AV} = average transmitted power, watts

$K = \left(\frac{1852 \text{ meters}}{\text{nautical mile}}\right)^4 = 11.76424 \times 10^{12}\ m^4/(n.m.)^4$

$(4\pi)^3 = 1984.40166$

B_n = receiver noise bandwidth, Hz

τ_c = compressed pulselength, seconds (sec)

$B_n\ \tau_c = 1$

$\left(\frac{S}{C+N}\right)_n$ = integrated signal-to-clutter + noise ratio required for a probability of detection (P_d) = 0.99 and a probability of false alarm (P_{fa}) = 10^{-10}. This is based on no signal fluctuation.

From Radar Detection by W. R. Rubin and J. V. DiFranco: Electro-Technology, April 1964, Science and Engineering Series #64, the $(\frac{S}{C+N})_n$ equals 16.0 dB. This is equivalent to a power ratio of 39.81.

L_T = Total system losses. Dependent on frequency and grazing angle. See Table III for losses.

N_o = receiver noise power, watts per Hz. Dependent on frequency. See Table IV.

R_s = slant range based on straight line approximation to the atmosphere. For detailed development, see Appendix B

$$= r_e \left[(1+\frac{h}{r_e}) \sin \psi - \sqrt{1 - (1+\frac{h}{r_e})^2 \cos^2 \psi} \right] \quad \text{n.m.} \qquad (2)$$

where

h = vehicle altitude, n.m.

r_e = earth radius = 3440 n.m.

ψ = depression angle measured from local horizontal at the radar platform.

$$= \arccos \left(\frac{r_e \cos \phi}{r_e + h} \right) , \text{ degrees} \qquad (3)$$

ϕ = grazing angle measured at the earth's surface, degrees

(PRF) = the pulse repetition frequency, for unambiguous range within a swath, pulses/sec

where

advantage has been taken of the radar platform altitude by transmitting just before the return from the near edge of the swath, such that sidelobe returns from below the radar platform occur at some time after the return from the far edge of the swath. This is the case, when $(R_{s_1} - R_{s_2}) \leq h$. See Figure A.

If $(R_{s_1} - R_{s_2}) > h$ use $(PRF) = \frac{C}{2 R_{s_1}}$ (4a)

If $(R_{s_1} - R_{s_2}) \leq h$ use $(PRF) = \frac{C}{2(R_{s_1} - h)}$ (4b)

C = speed of light = 1.61875×10^5 (n.m.)/sec

R_{s_1} = slant range to outer edge of swath, n. m.

R_{s_2} = slant range to inner edge of swath, n. m.

$$= \sqrt{r_e^2 + (r_e + h)^2 - 2 r_e (r_e + h) \cos (\alpha_o - \frac{W_G}{r_e})} \text{ , n.m.} \quad (5)$$

$$\alpha_o = \psi_o - \phi_o \text{ , degrees} \quad (5a)$$

ψ_o = equation (3) with $\phi = \phi_o$, degrees

ϕ_o = initial grazing angle, degrees

W_G = range swath width, n. m.

The above equation is developed in Appendix B.

$$G = \text{antenna gain} = \left(\frac{4 \pi H D}{\lambda^2}\right) \eta_a \qquad (6)$$

λ = wavelength, meters

H = physical height of the antenna

$$= \frac{72 \lambda}{\theta_{EO}} \text{ , meters} \qquad (7)$$

A vertical beamshaping factor (χ) is defined to permit consideration of modified and unmodified antennas. It is:

$$\theta_{EO} = \chi \theta_E \qquad 0 < \chi \leq 1 \qquad (8)$$

where χ represents that portion of the beamwidth that is unmodified

θ_{EO} = unmodified vertical beamwidth

θ_E = vertical beamwidth necessary to cover swath

$$= \psi_m - \psi_o \qquad (9)$$

The remaining portion ($(1 - \chi)\ \theta_E$) of the vertical pattern is covered by the use of beamshaping. As may be seen, the higher the value of χ the less beamshaping involved.

$$\psi_m = \arccos \left[\frac{r_e \sin \left(\alpha_o - \frac{W_G}{r_e} \right)}{R_{s_2}} \right] , \text{ degrees} \qquad (10)$$

D = physical length of the antenna

$$= \frac{72\ \lambda}{\theta_{AZ}} , \text{ meters} \qquad (11)$$

θ_{AZ} = azimuth beamwidth, degrees

η_a = aperture efficiency = 0.55

When no beamshaping is used ($\chi = 1$), the antenna is aimed so that the 3 dB points of the vertical pattern coincide with the far and near grazing angles. The gain used in determining the average power is:

$$G' = G\ (.501187) \qquad (12)$$

where .501187 represents the power ratio for 3 dB.

When beamshaping is used ($\chi < 1$), the antenna is aimed so that a 3 dB point of the vertical pattern coincides with the far grazing angle (ϕ_o).

The beamshaping function is:

$$\frac{\csc^2 \theta \cos \theta}{\csc^2 \theta_{EO} \cos \theta_{EO}} \qquad \text{for} \quad \theta_{EO} \leq \theta \leq \theta_E \tag{13}$$

In rewriting the numerator of equation (13) in terms of ψ, we obtain

$$\frac{\csc^2 (\psi - \psi_o) \cos (\psi - \psi_o)}{\csc^2 \theta_{EO} \cos \theta_{EO}} \qquad \text{for} \quad \psi_o + \theta_{EO} \leq \psi \leq \psi_o + \theta_E \tag{14}$$

In addition to the beamshaping function, there is a loss in gain due to the modification of the original antenna pattern to produce a $\csc^2 \theta \cos \theta$ pattern from θ_{EO} to θ_E.

This loss (G_o) is defined to be:

$$G_o = \frac{\theta_{EO}}{\theta_{EO} + \left(\frac{\sin \theta_E - \sin \theta_{EO}}{\sin \theta_E} \right) \tan \theta_{EO}} \tag{15}$$

It can be shown that when $\chi = 1$, $G_o = 1$ and for $\chi < 1$, $G_o < 1$.

The gain function used at the far point is:

$$G_{far} = \left(\frac{4\pi H D \eta_a}{\lambda^2}\right) (.501187) (G_o) \quad (16)$$

while the gain function used at the near point is:

$$G_{near} = \left(\frac{4\pi H D \eta_a}{\lambda^2}\right) (.50119) (G_o) \left(\frac{\csc^2 \theta_E \cos \theta_E}{\csc^2 \theta_{EO} \cos \theta_{EO}}\right) \quad (17)$$

To provide realistic antenna solutions and to limit the computer output, the following constraints are imposed:

Vertical Beamwidth

If $\theta_{EO} < 0.25$ degrees set $\theta_{EO} = 0.25$ degrees

If $\theta_{EO} \geq 0.25$ degrees continue solution using $\theta_{EO} = \chi \theta_E$

Physical Length

If $D > 500$ ft., solution not allowed, go on to next solution

If $D \leq 500$ ft., acceptable solution, continue

Antenna Aperture

If H D ≦ 15,000 sq. ft., acceptable solution, continue

If H D > 15,000 sq. ft., too large; set area back to 15,000 sq. ft.

then recalculate the antenna height using $\frac{15,000}{D} = H$

The following equations are an approximation to a curve in Fig. 2.8(a) from Introduction to Radar Systems by M. I. Skolnik, for the determination of the integration improvement factor ($S_i(n)$), when n pulses are integrated.

$$S_i(n) = 1.01\, n^{.944} \qquad 1 \leqq n < 4 \tag{18}$$

$$= 1.282n^{.775} \qquad 4 \leqq n < 20$$

$$= 1.675n^{.688} \qquad 20 \leqq n < 100$$

$$= 2.594n^{.593} \qquad n \geqq 100$$

$$n = (PRF)\, T_i \text{ , pulses}$$

T_i = the period of time that a target remains within the 3 dB azimuth beamwidth of the radar system, seconds

$$= 2\,(h + r_e)\sqrt{\frac{h + r_e}{GM_\Gamma}}\left[\arcsin\left(\frac{R_s \sin\left(\frac{\theta_{AZ}}{2}\right)}{(h + r_e) - R_s \sin\psi}\right)\right] \tag{19}$$

GM_E = gravitational constant = 6.2766×10^4 $(n.m.)^3/sec^2$

The above expression is developed in the Case III study report.

L_{FR} = loss in gain due to Faraday rotation. See Table I for values and Reference 2 for details concerning development of table.

σ_T = non-fluctuating target cross-section, specified to be 200 m^2

σ_c' = effective radar cross-section of sea clutter within a resolution cell

$$= K_1 \sigma^\circ R_s \theta_{AZ} \frac{C \tau_c}{2} \sec \phi \qquad (20)$$

K_1 = 3.4299×10^6 $m^2/(n.m.)^2$

σ° = backscatter coefficient as obtained from Fig. 2. Dependent on frequency and grazing angle.

C = 1.61875×10^5 $(n.m.)/sec$

ζ = Faraday rotation clutter coefficient. See Table II for values and Reference 2 for details concerning the development of the table.

$S_i(n_c)$ = modified integration improvement factor to account for partial correlation of sea clutter. When T_d (PRF) ≤ 1 no correlation between pulses, use n in $S_i(n)$ eqn. When T_d (PRF) $\geq i$ partial correlation between pulses, use n_c in $S_i(n)$ eqn.

where T_d = decorrelation time

$$= \frac{K_s \lambda}{\theta_{AZ}} \sqrt{\frac{r_e + h}{G_{ME}}} \qquad (21)$$

K_s = 1,852 m/n.m.

n_c = number of independent pulses returned from clutter

$$= \frac{n}{T_d \ PRF} \text{ , pulses} \qquad (22)$$

P_t = peak transmitted power, watts (computed, but not used in the solution of the radar equation)

$$= \frac{P_{AV}}{\tau_c \ (PRF)} \quad \frac{\tau_c}{\tau} \qquad (23)$$

τ = transmitted pulselength, sec.

$\frac{\tau}{\tau_c}$ = pulse compression ratio = 100 for this study

PRF TIMING

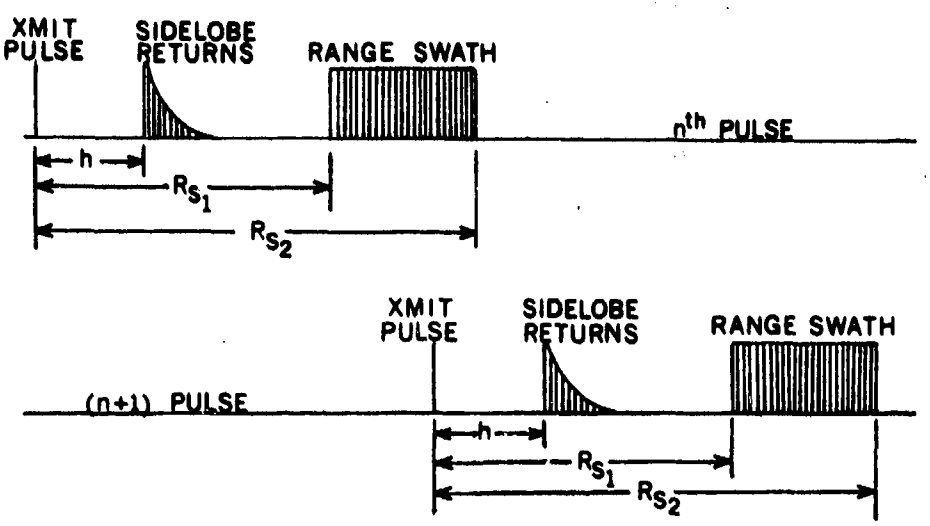

$$R_{s_2} - R_{s_1} > h$$

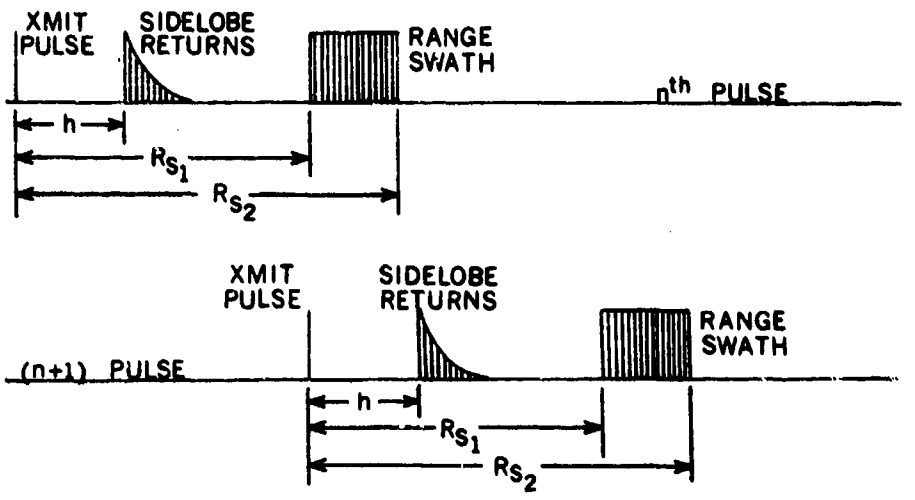

$$R_{s_2} - R_{s_1} \leq h$$

FIGURE A

VERTICAL BEAMSHAPE

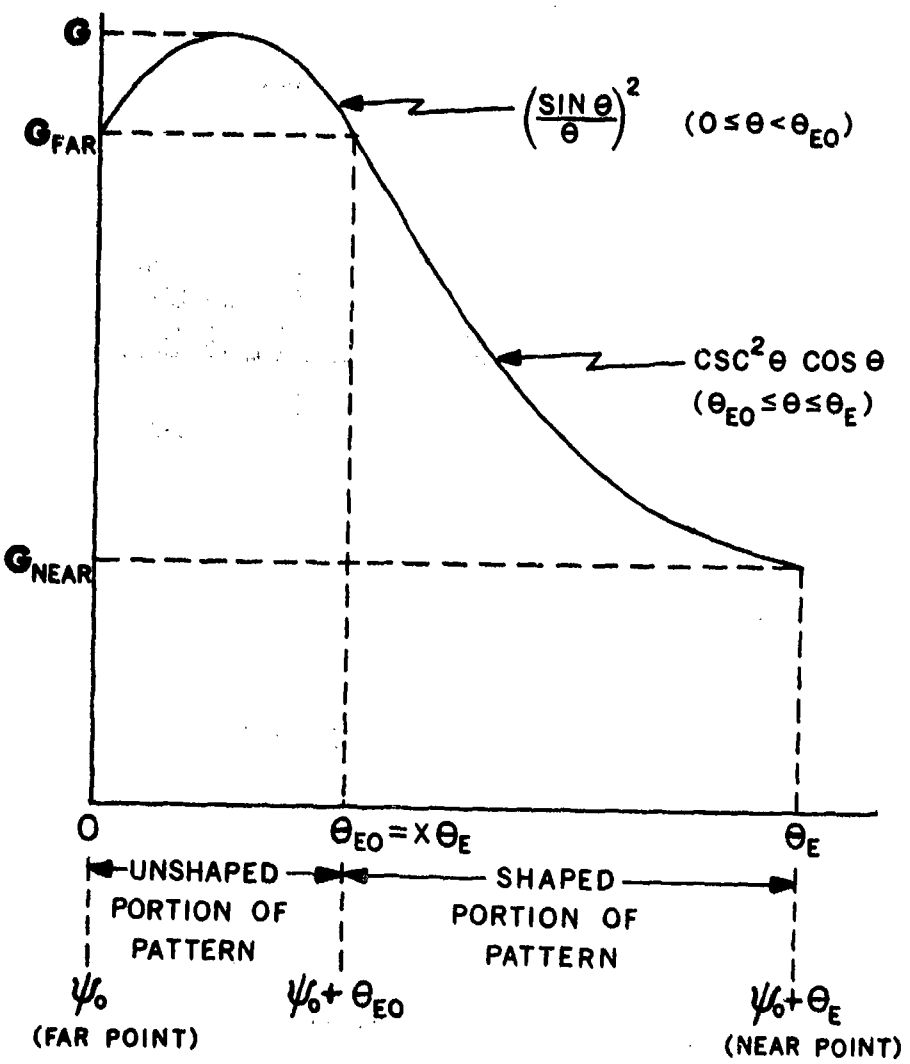

FIGURE B

APPENDIX B

GEOMETRICAL RELATIONSHIPS BETWEEN HEIGHT, SLANT RANGE, DEPRESSION ANGLE AND GRAZING ANGLE FOR AN AIRBORNE RADAR SYSTEM

(U) The following expressions illustrate the geometrical relationships between height, slant range, depression angle and grazing angle for the side-looking radar case.

(U) It should be noted that atmospheric bending effects have been neglected; straight lines have been used for the ray paths, as may be seen by looking at Fig. 1 .

From Fig. 1 .

$$W_G = r_e \ (\alpha_o - \alpha_m) \qquad (1)$$

where α_o and α_m are in radians

The only unknown quantity in (1) is α_m

Solving for α_m

$$\alpha_m = \alpha_o - \frac{W_G}{r_e} \qquad (2)$$

(U) Applying the law of sines to Fig. 1 , the result is:

$$\frac{R_s}{\sin \alpha} = \frac{r_e}{\sin (90 - \psi)} = \frac{r_e + h}{\sin (90 + \phi)} \qquad (3)$$

where $\alpha_m \leq \alpha \leq \alpha_o$

$\psi_m \leq \psi \leq \psi_o$

$\phi_o \leq \phi \leq \phi_m$

however:

$$\alpha = 180° - (\phi + 90°) - (90 - \psi) \qquad (4)$$

simplifying (4)

$$\alpha = \psi - \phi \qquad (5)$$

Substituting (5) into (3) remembering that

$$\sin (90 \pm X) = \cos X$$

$$\frac{R_s}{\sin (\psi - \phi)} = \frac{r_e}{\cos \psi} = \frac{r_e + h}{\cos \phi} \qquad (6)$$

$$\cos \psi = \frac{r_e \cos \phi}{r_e + h} \qquad (7)$$

$$\psi = \arccos \left(\frac{r_e \cos \phi}{r_e + h} \right) \qquad (8)$$

The maximum value of (8) that can be used occurs when $\phi = 0$, which is the radar horizon.

$$\psi_{hor} = \arccos \left(\frac{r_e}{r_e + h}\right) \tag{9}$$

Solving (6) for R_s

$$R_s = \frac{r_e \sin (\psi - \phi)}{\cos \psi} \tag{10}$$

However:

$$\sin (A - B) = \sin A \cos B - \cos A \sin B \tag{11}$$

Using (11) in (10)

$$R_s = \frac{r_e [\sin \psi \cos \phi - \cos \psi \sin \phi]}{\cos \psi} \tag{12}$$

(U) Rearranging (7)

$$\cos \phi = \left(1 + \frac{h}{r_e}\right) \cos \psi \tag{13}$$

Substituting (13) into (12) and cancelling

$$R_s = r_e \left[\left(1 + \frac{h}{r_e}\right) \sin \psi - \sin \phi\right] \tag{14}$$

The maximum value of (8) that can be used occurs when $\phi = 0$, which is the radar horizon.

$$\psi_{hor} = \arccos \left(\frac{r_e}{r_e + h}\right) \tag{9}$$

Solving (6) for R_s

$$R_s = \frac{r_e \sin (\psi - \phi)}{\cos \psi} \tag{10}$$

However:

$$\sin (A - B) = \sin A \cos B - \cos A \sin B \tag{11}$$

Using (11) in (10)

$$R_s = \frac{r_e [\sin \psi \cos \phi - \cos \psi \sin \phi]}{\cos \psi} \tag{12}$$

(U) Rearranging (7)

$$\cos \phi = \left(1 + \frac{h}{r_e}\right) \cos \psi \tag{13}$$

Substituting (13) into (12) and cancelling

$$R_s = r_e \left[\left(1 + \frac{h}{r_e}\right) \sin \psi - \sin \phi\right] \tag{14}$$

where sin ϕ can be represented as:

$$\sin \phi = \sqrt{1 - \cos^2 \phi} \tag{15}$$

Substituting (13) into (15)

$$\sin \phi = \sqrt{1 - \left[\left(1 + \frac{h}{r_e} \right) \cos \psi \right]^2} \tag{16}$$

Substituting (16) into (14)

$$R_s = r_e \left[\left(1 + \frac{h}{r_e} \right) \sin \psi - \sqrt{1 - \left[\left(1 + \frac{h}{r_e} \right) \cos \psi \right]^2} \right] \tag{17}$$

(U) The angle ψ_m is needed to determine the elevation angle ($\theta_E = \psi_m - \psi_o$) for a given swath width (W_G). Equation (17) cannot be used, since both R_{s_3} and ψ_m are unknown. Therefore, the law of cosines will be used on Fig. 1 .

$$R_{s_2} = \sqrt{r_e^2 + (r_e + h)^2 - 2 r_e (r_e + h) \cos \alpha_m} \tag{18}$$

Substituting (2) into (18)

$$R_{s_2} = \sqrt{r_e^2 + (r_e + h)^2 - 2 r_e (r_e + h) \cos \left(\alpha_o - \frac{W_G}{r_e} \right)} \tag{19}$$

(Page 56 is Blank)

where:

$$\alpha_o = \psi_o - \phi_o \tag{5}$$

or using (8)

$$\alpha_o = \arccos\left(\frac{r_e \cos \phi_o}{r_e + h}\right) - \phi_o \tag{20}$$

SECRET

Security Classification

DOCUMENT CONTROL DATA - R & D

(Security classification of title, body of abstract and indexing annotation must be entered when the overall report is classified)

1. ORIGINATING ACTIVITY *(Corporate author)*

Naval Research Laboratory
Washington, D.C. 20390

2a. REPORT SECURITY CLASSIFICATION

SECRET

2b. GROUP

3

3. REPORT TITLE

OCEAN SURVEILLANCE RADAR PARAMETRIC ANALYSIS
CASE II - NONCOHERENT SIDELOOKING RADAR (U)

4. DESCRIPTIVE NOTES *(Type of report and inclusive dates)*

An interim report on one phase of the problem.

5. AUTHOR(S) *(First name, middle initial, last name)*

Stephen Angyal, Donald F. Hemenway, and Steve A. Zuro

6. REPORT DATE	7a. TOTAL NO. OF PAGES	7b. NO OF REFS
April 1968	62	5

8a. CONTRACT OR GRANT NO.	9a. ORIGINATOR'S REPORT NUMBER(S)
NRL Problem 53R02-46	
b. PROJECT NO. A37538-006/6521/F019-02-01	
c.	9b. OTHER REPORT NO(S) *(Any other numbers that may be assigned this report)*
d.	

10. DISTRIBUTION STATEMENT

In addition to security requirements which apply to this document and must be met, each transmittal outside the agencies of the U.S. Government must have prior approval of Director, Naval Research Laboratory, Washington, D.C. 20390.

11. SUPPLEMENTARY NOTES	12. SPONSORING MILITARY ACTIVITY
	Department of the Navy (Naval air Systems Command - Astronautics Division) Washington, D.C. 20360

13. ABSTRACT

(Secret)

(S) A computer-aided analysis of the Non-Coherent Sidelooking Radar (Case II) for Ocean Surveillance shows trends in system requirements as functions of radar system and operational parameters. The parameters specifically analyzed include: Operating frequency, pulse length, swath width, azimuthal beamwidth, orbital altitude, antenna size, average and peak power, elevation beamshaping, and swath position relative to different outer-bound grazing angles.

(U) In the development of the radar equation for the Case II analysis, consideration is given to: Sea clutter models, tropospheric propagation losses, system losses, Faraday rotation effects, target integration, and partial sea-clutter integration effects.

14. KEY WORDS	LINK A		LINK B		LINK C	
	ROLE	WT	ROLE	WT	ROLE	WT
Sidelooking Radar						
Non-Coherent Sidelooking Radar						
Radar Parametric Analysis						
Radar Equation Computer Program						
Radar Systems Analysis						

UNITED STATES GOVERNMENT

memorandum

DATE: September 9, 1996

REPLY TO ATTN OF: Code 5304

SUBJECT: Declassification of NRL Memorandum Reports 1874 and 1966, Request for

TO: 1221.1

1. This memorandum is to request that the security classification of the two reports listed below be changed from a current classification of **CONFIDENTIAL** to **UNCLASSIFIED**.

NRL Memorandum Report 1874
Ocean Surveillance Radar Parametric Analysis
Case II - Noncoherent Sidelooking Radar
(Unclassified Title)
S. Angyal, D. F. Hemenway, and S. A. Zuro
April 1968

AD-391 513

NRL Memorandum Report 1966
Ocean Surveillance Radar Parametric Analysis
(Unclassified Title)
Final Report
E. N. Carey, R. L. Eilbert, R. E. Ellis, D. F. Hemenway and A. E. Leef
March 1969.

AD-501 065

2. The above reports are more than 27 years old, and as one of the authors, I can see no need for continuing to maintain any classification on the subject studies, and recommend that they be designated as **UNCLASSIFIED** reports.

3. The above information was submitted to Code 1221.1 on a memorandum dated September 4, 1996. This re-submission is for the purposes of including the following statement :

> Further, this memorandum requests that the subject reports be approved for public release: distribution unlimited.

Donald F. Hemenway
Code 5304

Completed
2-7-2000
B.W.

OPTIONAL FORM NO. 10
(REV. 1-80)
GSA FPMR (41 CFR) 101-11.6
5010-114

★U.S. GPO: 1989-241-175/90096